Structures 32 (2021) 474–493

Contents lists available at ScienceDirect

Structures

journal homepage: www.elsevier.com/locate/structures

Structure soil structure interaction of conventional and base-isolated building subjected to real earthquake

Srijit Bandyopadhyay [a,b,*], Y.M. Parulekar [a,b,*], Aniruddha Sengupta [c], J. Chattopadhyay [a,b]

[a] Homi Bhabha National Institute, Mumbai 400094, India
[b] Reactor Safety Division, Bhabha Atomic Research Center, Mumbai 400085, India
[c] Department of Civil Engineering, Indian Institute of Technology, Kharagpur, West Bengal 721302, India

ARTICLE INFO

Keywords:
Soil structure interaction
Real earthquakes
Base isolators
Dynamic analysis

ABSTRACT

In this paper, the effect of structure soil structure interaction of the two adjacent Reinforced Concrete (RC) three storied structures, located in highest seismic zone of India are studied. One of the buildings is mounted on base isolator (Lead Rubber Bearing) and the other building is a normal conventional RC framed structure. The buildings were instrumented and real earthquake response of the buildings was captured during the period 2006 to 2007. The frequency of the base isolated structure was lesser than the conventional structure by a factor of 2.6 and the response was also reduced by factor of 4 to 5 as envisaged. However, structure soil structure interaction was observed in the response of the base isolated building and the measured response showed the frequency of the nearby structure. A numerical simulation considering two adjacent structures together with detailed soil modelling is performed and the numerical results are validated with recorded real earthquake data. Furthermore, response of both the buildings are studied with the larger earthquake in the same area with a PGA of 0.26 g and the response acceleration of the base isolated building is reduced by about 4.1 times the conventional building response. Moreover, the floor spectra of the roof of base isolated structure has multiple peaks due to nonlinear deformation of the isolator which gives different effective stiffness for different displacements in the hysteretic deformation of the isolator experienced during cyclic motion. It is also observed that that frequency of the base isolated building reduces with increasing peak ground acceleration.

1. Introduction

Earthquakes cause disastrous impact when they occur in a densely populated area with closely spaced structures. Many devastating earthquakes, such as Nepal Earthquake (2015) and Bhuj earthquake (2001), occurred in the past have caused lot of damage to the structures. These earthquakes have led to development of rational theories for failure mechanisms of different types of structural configurations. Seismic design of structures is one of the most important and challenging issues to the structural engineers. The general aim in seismic design is to increase the structural capacity against earthquakes using shear wall, braced frame and moment frames. But all these arrangements increase the storey acceleration and inter storey drift. As a result, many a times it is observed that non-structural elements are severely damaged during strong earthquakes. Seismic isolation is one of the effective method of protecting the buildings from major earthquake damage.

The seismic base isolation method has been studied and applied to buildings since 1980′s. Base isolation [1–4] is aseismic design approach in which the structural fundamental frequency of vibration is reduced to a value lower than the predominant energy-containing frequencies of the earthquake ground motion. Base isolation system decouples the structure from the horizontal components of the earthquake ground motion by interposing a layer with low horizontal stiffness between the structure and the foundation. Since last few decades, several base isolator devices have been studied to isolate the main structure from the ground shaking, such as friction pendulum system (FPS), lead rubber bearings, laminated rubber bearing etc[5–7].

One of the most common base isolator, the Lead Rubber Bearing (LRB) is used in the present work. This isolator was developed by Kelly and Hodder [8] in 1981 and it consists of multiple layers of thin rubber sheets and reinforcing steel plates with a central core of solid lead plug. The lead plug is used basically to absorb earthquake energy and reduce the displacements. Base isolators which were installed in various structures like bridges and hospitals were studied by researchers like Hameed et. al [9] in 2008 and Nagarajaiah and Xiaohong [10] in 2000

* Corresponding authors at: Reactor Safety Division, Bhabha Atomic Research Center, Mumbai 400085, India.
E-mail addresses: srijit@barc.gov.in (S. Bandyopadhyay), yogitap@barc.gov.in (Y.M. Parulekar).

https://doi.org/10.1016/j.istruc.2021.03.069
Received 20 November 2020; Received in revised form 8 March 2021; Accepted 10 March 2021

Nomenclature

σ_{YL}	The theoretical yield strength for lead
A_L	The cross sectional area of lead
K_1	Initial stiffness of the base isolator
K_2	The post yield stiffness
$G_{0.5}$	Shear modulus of rubber at 50% strain
Σt	Total rubber thickness
A_R	Cross sectional area of rubber
F_y	yield force of lead core.
Δ_y	yield displacement of lead core.
E_m	Modulus of elasticity of unreinforced masonry infill
E_f	Modulus of elasticity of Moment Resisting Frame (MRF)
I_c	Moment of inertia of the adjoining column.
Θ	Angle of diagonal with horizontal
A_e	Area of strut
W_m	the width of equivalent strut
t	the thickness of the infill wall
L	the length of the infill diagonal
h	floor to floor height of the building.
G_{max}	Initial shear modulus,
γ_r	the reference strain,
h_{max}	The maximum damping.
V_s	Shear wave velocity.
ρ	Density.
l_{ele}	vertical size of the element,
V_s	shear wave velocity of the layer
f_{max}	the cutoff frequency of the analysis

respectively.

The effect of eccentricity of the structure when supported on base isolator is studied by Ryan and Chopra [11] considering the structures as a fixed base. However, the assumption of fixed base is only valid when structure is founded on rock or soil with high stiffness. In general, soil structure interaction (SSI) reduces the structural frequency and modifes the energy dissipation in terms of material damping and radiation damping of the soil [12]. Equation of motion of building system considering SSI was formulated by Novak and Henderson [13] and they showed that the frequency of the structure is reduced due to the SSI. Coupled effects of base isolated structure and soil structure interaction has gained importance among the researchers since the last two decades. Earlier, analytical studies were conducted on effects of base isolated structures with SSI. In 2003, Tongaonkar and Jangid [14] studied the response of the base isolated bridges considering SSI effects and they recommended to incorporate SSI in design of base isolated bridges especially when flexibility of base isolator and soil are comparable. In 2016, Krishnamoorthi and Anita [15] studied soil structure interaction of FPS isolated structure using finite element model. They concluded that SSI affects the response of structure isolated with FPS and mostly the response increases due to SSI. Recently in 2020, Tsiavos et. al. [16] investigated the effect of deformable sliding layer on the dynamic response of seismically isolated structures. They found that deformable sliding layer is beneficial for seismic and vibration isolation of structures as it leads to significant reduction of their maximum acceleration response compared to rigid plastic sliding layer case. Shake table tests were also conducted by researchers to study the effect of SSI on base isolated structures. Li et. al. [17] investigated the response of high rise base-isolated structure on soft soil by performing shake table tests. It was reported that natural frequency of base isolated structure is less than the same system without considering SSI. Zhuang et.al. [18] performed shaking table test to estimate the effect of SSI on the dynamic characteristics of a base-isolated structure situated on a multi-layered soil foundation including a soft clay layer. They found the isolation efficiency of the isolator is reduced by the SSI effects, especially with increasing peak ground acceleration (PGA) of the input motion. They also reported that damping ratio of the base isolated system considering SSI is more than that of the same system without considering SSI. The work on developing simplified model of Soil-structure interaction for seismically isolated containment buildings in Nuclear Power Plant was carried out by Ashiquzzaman and Kee-Jeung Hong [19] in 2016. Recently in 2020, Almansa et.al. [20] conducted a case study on suitability of base isolation system on RC building founded in soft soil in Shanghai. They reported in their study that, the base isolator is most suitable for medium height structures if founded on soft soil. In 2020, Radkia et al. [21] investigated the effects of seismic isolators on steel asymmetric structures considering soil-structure interaction. They showed that for different types of soils the displacement and slipping speed of isolators decreased for all the twenty four different models of the structures studied. The results also suggested that substructure soil typology had a significant effect on the design parameters of isolators. Similar findings are also observed in other literatures [22,23].

It is thus evident that large amount of study has been carried out on base isolators with various types of soils and their interactions. Nevertheless, a systematic study on two actual instrumented buildings located on soft soil strata one with base isolator and the other on a conventional foundation subjected to real earthquakes is not available till date. This study is essential as in most of the cities, structures are closely spaced and it often occurs that the base isolated structure is situated near the conventional structure. Hence, the knowhow in the behavior of the closely spaced base isolated structure and conventional structure situated on soft soil subjected to earthquake loads is very essential to be gained. The complexity of the problem needs to be studied by modeling the structures with soil and performing detailed time history analysis. Moreover, numerically studying the response of these structures subjected to real earthquake and comparing it with the real time measured response will give a proper validation of the problem. Unlike soil structure interaction very limited amount of data is available regarding structure soil structure interaction (SSSI).

Earlier, mostly only analytical studies were performed by researchers [24–27] on this topic of SSSI. They conducted numerical analyses of 3D structural models with soil for studying SSSI and reported that various factors such as relative foundation sizes, distance between the structures, relative stiffness of the structures and soil are responsible for SSSI. Recently, Bolisetti and Whittaker [28] conducted centrifuge tests to study SSSI and reported no influence of SSSI in the building responses while Kirkwood and Dashti [29] conducted centrifuge tests on both far spaced and closely spaced structures to identify how the building separation and ground motion characteristics affect the response of adjacent structures founded on a layered, liquefiable soil profile. They concluded that properly planned configurations may be employed in addition to traditional mitigation strategies, to improve the settlement-rotation response of adjacent structures. Celebi [30] showed the effects of SSSI in adjacent buildings, from the recorded earthquake data of 1987 Whittier-Narrows earthquake. From the study, he concluded that response of the building and near-by surface response was affected due to SSSI. He also observed considerable changes in structural response in specific frequencies. Till date, study of SSSI based on actual field data of real earthquake with one building on base isolator and other on conventional foundation is not conducted. Hence in the present paper, a novel work of studying the effect of the vibration response of two adjacently located and differently founded structures using the real earthquake response measurement and its analytical simulation is presented.

The present study is carried out on two RC framed buildings, which are located in one of the highest seismicity prone region of India

(Guwahati Region). One of the RC framed structure is placed over lead rubber base bearing (LRB) and other building is a conventionally founded structure. The two buildings considered were instrumented and monitored during the period 2006 to 2007, which lead to capturing of two real earthquakes and procuring their respective data. The instrumented buildings are located close to each other at a separation distance of 2.2 m. The effect of structure soil structure interaction due to these earthquakes is simulated numerically and the response obtained is validated with measured earthquake response. Moreover, response of the buildings with design basis earthquake of the study region is also obtained.

2. Building and subsoil description

Two adjacent three storied buildings with typical floor plan, one with conventional and other one with base isolated foundation resting on subsoil, are located in the Guwahati region of India. The building which is founded on isolated footing, is described as conventional building in the present paper. Latitude and longitude of Guwahati location is 26.1903° N, 91.6920° E. As per the seismic code of India, Guwahati falls into the high seismic zone (Zone V) [31]. The buildings consist of reinforced concrete (RC) frame structures with brick infill walls. The plan and elevation of the structures are shown in Fig. 1(a) and isometric view of the buildings along with isolator position for one structure is shown in Fig. 1(b). Each building has a plan area with 4.5 m length and 3.3 m width. The floor to floor height of both the buildings is 3.3 m. There are four corner columns rectangular in shape and these have width of 0.3 m and depth of 0.4 m. The dimensions of the beams are 0.45 m depth and 0.25 m width. The thickness of the RC slab is 0.15 m. Two buildings are separated with a distance of 2.2 m. The buildings were

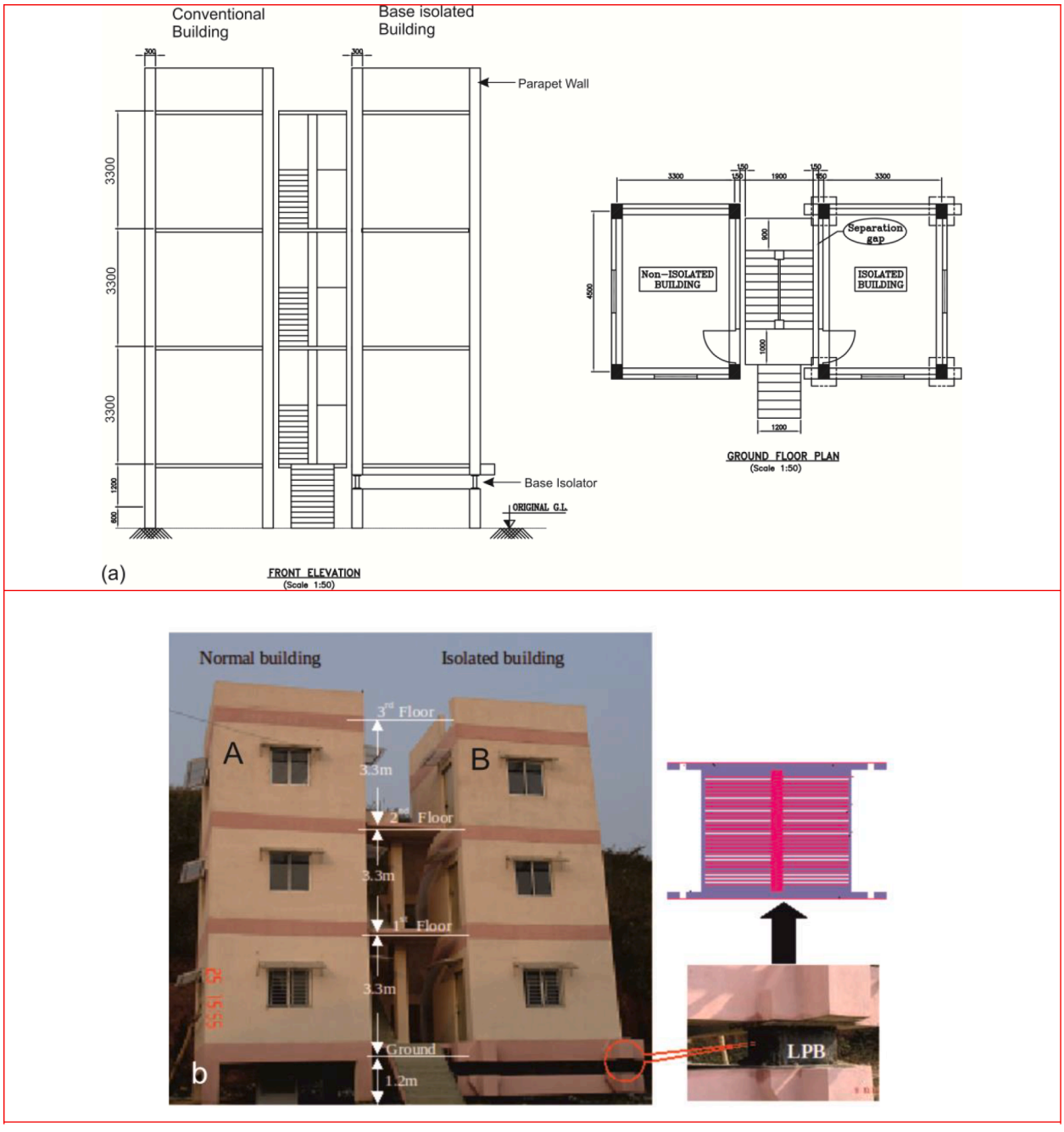

Fig. 1. (a) Plan and elevation of conventional and isolated building showing position of isolators; (b) Isometric view of the buildings located in Guwahati.

fully instrumented and the earthquake data was recorded. During 2006–07, the base isolated building was placed over lead rubber bearing base isolators, which were located in between plinth level and ground floor level. In actual construction procedure, the foundation of both the buildings were placed 1.5 m below the surface. Basu et.al. [32] has performed an extensive study of soil amplification in the same region and shear wave velocity profile obtained by them is used for the present study. Details of shear wave velocity profile is shown in Fig. 2. It is reported that the soil upto 15 m is mostly soft or loose with SPT-N value less than 30. It is observed from Fig. 2, that the mean shear wave velocity upto first 5 m varies from 100 m/s to 120 m/s and in next 10 m it uniformly increases to 300 m/s.

3. Base isolator

Actual location of Lead Rubber Bearing (LRB) isolator in the base isolated building is shown in Fig. 1(b). Four numbers of bearings are placed below the four columns in between ground floor level and plinth beam and the location of isolators in plan and elevations are shown in Fig. 1(a). Lead rubber bearing has alternate layers of rubber and steel with a central lead energy dissipating core. The rubber in the isolators acts as a spring. It is very soft laterally but very stiff vertically. The high vertical stiffness of the isolator is achieved by having thin layers of rubber reinforced by steel shims. These two characteristics allow the isolator to move laterally with relatively low stiffness and yet carry significant axial load due to their high vertical stiffness. Lead rubber bearing contains a lead plug at the center to dissipate hysteretic energy. Lead rubber bearing has dimension of 460 mm × 460 mm in plan, and 355 mm in height with alternate layers of 29 numbers of 7 mm thick rubber and 28 numbers of 4 mm thick steel plates. Moreover, in lead rubber bearing at the central location, 55 mm diameter lead core is used. A schematic diagram of base isolator is shown in Fig. 3. Specification of lead rubber isolator is given in Table 1. Before placing the isolator at the foundation location of the base isolated building, the cyclic test of base isolator was conducted at Structural Engineering Laboratory of IIT Guwahati using servo-controlled hydraulic MTS actuators with 100 T capacity in 2004. The details of the tests are mentioned in Deb and Dutta [33]. Cyclic load deformation curve of lead rubber bearing obtained from the tests is shown in Fig. 5. Details of lead rubber bearing are explained in Dubey et al. [34] and Nath et al. [35]. When lead rubber is subjected to low lateral loads, which are specifically due to wind, the LRB is stiff both laterally and vertically. The lateral stiffness results from the high elastic stiffness of the lead plug and vertical rigidity. At higher lateral load level, the lead yields and the lateral stiffness of the bearing is significantly reduced and period shift is observed [8]. Cyclic behavior of the lead rubber isolator is also simulated with numerical software, MIDAS GTS NX [36] by modeling only the lead rubber base isolator as a nonlinear general link element. Bilinear hysteretic model is used as link property to simulate the isolator hysteretic behavior. The load deformation shape of LRB subjected to cyclic loading is represented as bilinear curve with an elastic stiffness (K_1) and post elastic stiffness (K_2) as shown in Fig. 4. The post yield slope (K_2) value is obtained from the properties of rubber and dimension of the isolator as given in Eq. (2) and is input as the FE model link element property. The initial stiffness K_1, obtained from the tests performed is also input and a symmetric yield function of normal bilinear hysteresis model is generated using horizontal sinusoidal loading with peak displacement of 120 mm. The hysteretic behavior of numerical link element is compared with experimental results and is shown in Fig. 5. The flexibility of rubber shifts the natural period of the structure which results in reduced seismic forces, and the plastic behavior of lead absorbs seismic energy. The force intercept at zero displacement is denoted as characteristic strength (Q_d). The characteristic strength is evaluated on the basis of the lead cross sectional area using Eq. (1), [8]

$$Q_d = \sigma_{YL} \times A_L \tag{1}$$

Where, σ_{YL} is the theoretical yield strength for lead which is 11 MPa.
A_L is the cross sectional area of lead.

The post yield stiffness, K_2, is equal to the stiffness of elastomeric bearing alone. $K_2$is calculated as per Eq. (2). [8]

$$K_2 = \frac{G_{0.5} A_R}{\sum t} \tag{2}$$

Where,
$G_{0.5}$ = Shear modulus of rubber at 50% strain
Σt = Total rubber thickness
A_R = Cross sectional area of rubber

The post yield stiffness, K_2 is calculated from the design parameters given in Table 1 and by substituting the parameters in Eq. (2). The value of K_2 thus obtained is 0.82 kN/mm. This value exactly matches with that obtained from the experimentally obtained hysteretic curve shown in Fig. 4. Using a linear relationship between initial stiffnessK_1 and post yield stiffness K_2 the value of the multiplier constant to obtain K_1 is calculated from the experiment and is reported in Eq (3) as 8.7. Kelly and Hodder [8] reported this value as 25 as they obtained K_1 as 25 times of K_2 in their study. This value of K_1 is thus isolator specific and is generally obtained from the tests once the value of K_2 is calculated.

$$K_1 = 8.7K_2 \tag{3}$$

Using Fig. 5, the shear force$F$, in the bearing at any specified displacement Δ is evaluated using the relations Eq. (4).

$$F = Q_d + K_2\Delta \tag{4}$$

Initial yield force of lead rubber bearing is denoted by $F_y$and corresponding yield displacement of lead core is represented by Δ_y. The initial yield force, F_y, is calculated from Eq. (4) and is shown in Eq. (5).

$$F_y = Q_d + K_2\Delta_y \tag{5}$$

From Fig. 5, it is also observed initial yield force F_y, can be represented as Eq. (6).

$$F_y = K_1\Delta_y \tag{6}$$

From Eqs. (5) and (6), yield displacement of lead rubber isolator is represented in terms initial yield stiffness and post yield stiffness and shown in Eq. (7).

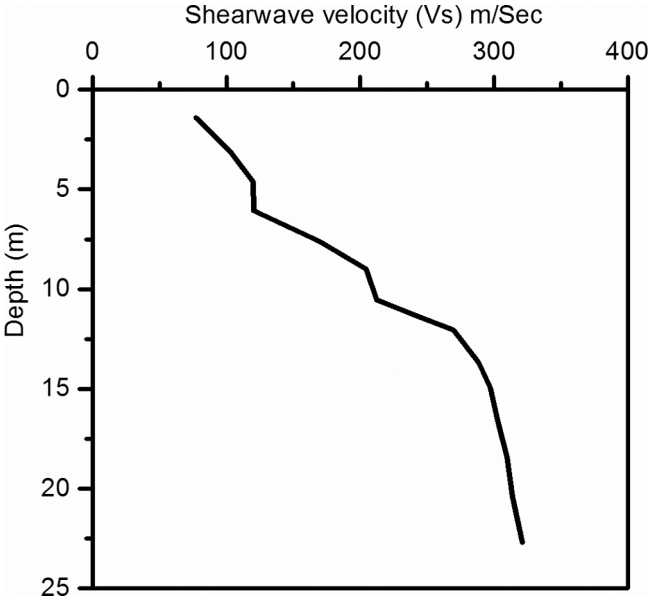

Fig. 2. Shear wave velocity profile of the study area [32].

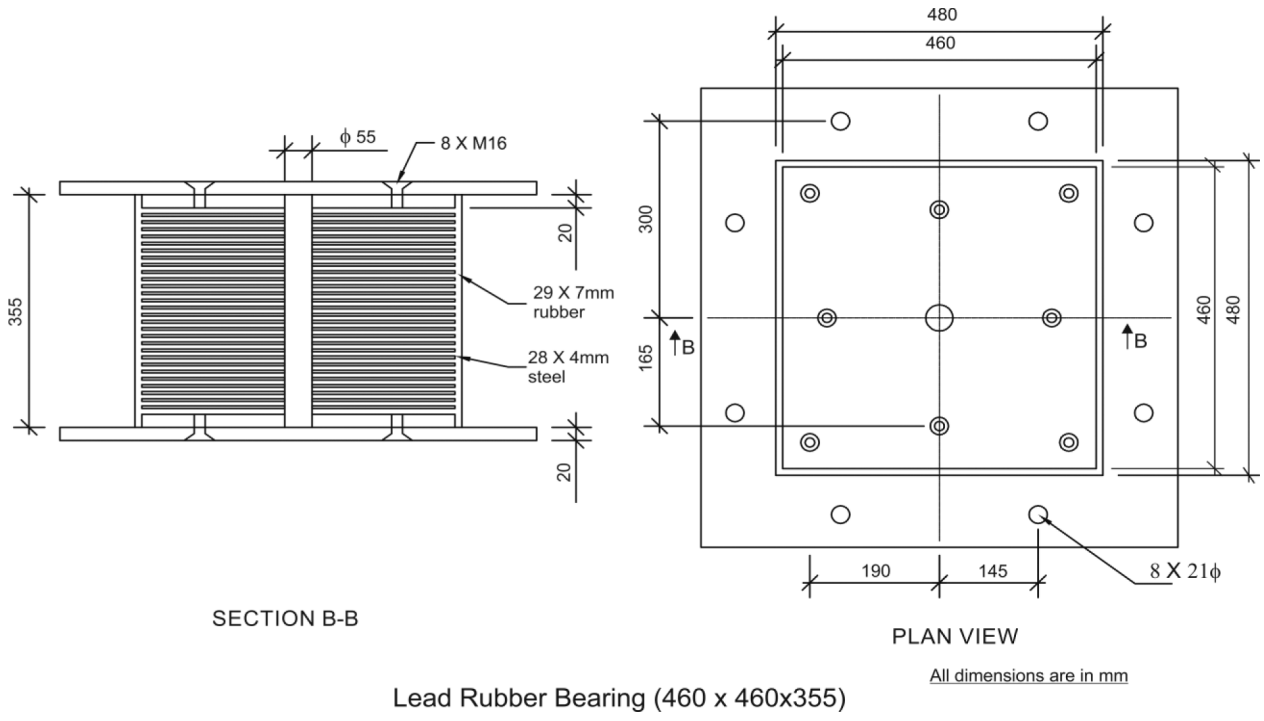

Fig. 3. Schematic diagram of lead rubber bearings and high damping rubber bearings.

Table 1
Specification of Lead rubber base isolator.

Isolator Parameters	Value
Shim dimension (mm)	460.0
Side cover thickness (mm)	10.0
Rubber G (Mpa)	0.8
Rubber layer thickness, t (mm)	7.0
Number of rubber layers	29
Shim plate thickness (mm)	4
End Shim Thickness (mm)	20
Lead Core Diameter (mm)	55
No of Lead core	1
Design Displacement (mm)	200
Equivalent Damping ratio %	>10

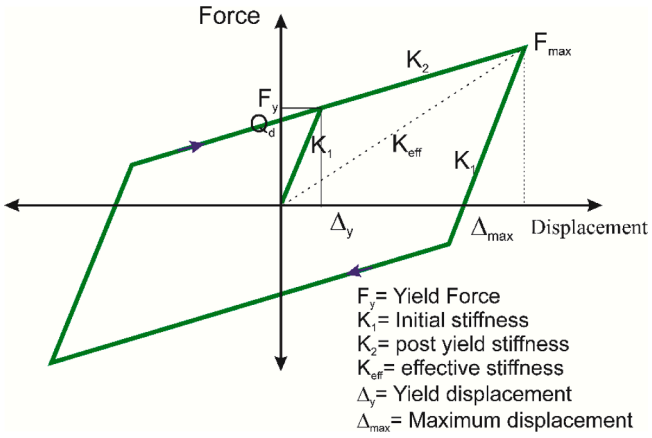

Fig. 4. Simplified characteristics of Lead Rubber Bearing.

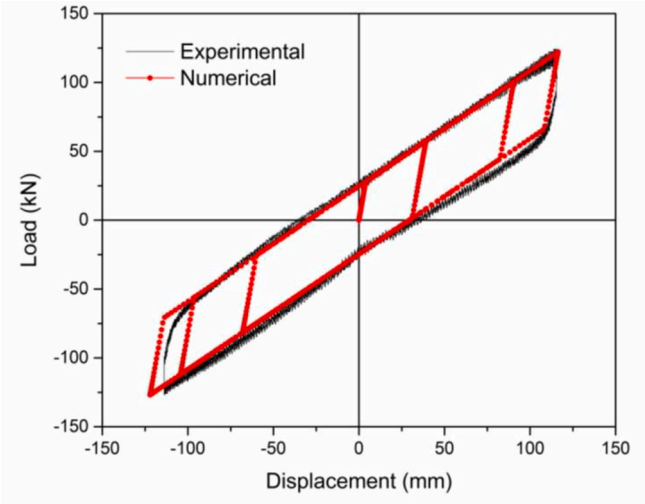

Fig. 5. Load deformation curve of lead rubber bearing.

$$\Delta_y = \frac{Q_d}{K_1 - K_2} \tag{7}$$

Using the isolator dimensions shown in Table 1 and the material properties of isolator, the load deformation curve is evaluated. The values of isolator parameters are obtained as follows:

Initial Stiffness $K_1 = 7.1$ kN/mm, $K_2 = 0.82$ kN/mm$\Delta_y = 4.1$ mm, Characteristic strength $= Q_d = 26$ kN and the ratio of post-yield stiffness to elastic stiffness (r) $= 0.11$, Yield force $F_y = 29$ kN.

4. Instrumentation of building

Both the buildings are instrumented with accelerometers to record their response under earthquakes. A twelve channel dynamic structural recording system with GPS and 32 MB PCMCIA card has been employed for recording the seismic ground motion and structural response of the

conventional and base-isolated buildings [33,35]. One surface tri-axial force balance accelerometer has been installed on the ground to capture earthquake induced ground motion. Four uni-axial accelerometers are installed in conventional building. Two of them are installed at ground floor level and other two at roof level of conventional building in two orthogonal directions. In addition to these, two more uni-axial accelerometers are placed at roof level of base isolated building to measure responses in orthogonal directions. One tri-axial accelerometer is placed at ground floor level of base isolated building. Earthquake motion recorded by the accelerometer in parallel to the longer direction of the building is mentioned as longitudinal direction motion and orthogonal to this longitudinal direction is mentioned in this paper as transverse direction motion. Fig. 6 shows the position of the sensors (in plan) at the ground floor and roof level of the prototype buildings. In the Fig. 6, 'U' denotes uniaxial accelerometer and 'T' denotes triaxial accelerometer. The details of location of these 12 recording channels and the index used to represent each of these in the present work are given in Table 2. Apart from building instrumentation, additional three records are measured away from the building and three records are measured below the conventional building.

A frequent occurrence of minor earthquake shaking is common in the Guwahati region [37]. However, earthquakes with M > 4 had enough intensity to trigger the recording systems installed in the test buildings. This paper deals with the behavior of the concerned structures under the influence of two earthquakes recorded during the period 2006 to 2007. One of the earthquake occurred on 6th Nov., 2006 and other one occurred on 29th Nov., 2007.

Earthquake recorded on 6th Nov. 2006 occured in Indo Myanmar border region at a focal depth of 120.8 km. The local magnitude of this earthquake was 4.8 Mb and distance of epicenter (24.694°N 95.146°E) from site was 385 km. Earthquake recorded on 29th Nov., 2007 occurred in Indo Myanmar border region at a focal depth of 114.8 km. The local magnitude of this earthquake was 5.1 Mb and distance of epicenter (23.390°N, 94.675°E) from site was 433 km. The analytical simulation of earthquake response obtained in vertical direction is not performed in the present work. The emphasis is only laid on the horizontal motion of earthquake response. Also, due to technical difficulties, ground floor data of conventional building was not available for earthquake recorded on 6th Nov., 2006.

5. Free vibration characteristics of the two structures

Finite element model of each structure is prepared in general purpose finite element software MIDAS GTS NX [36]. Buildings consists of beams and columns which are modeled as frame elements. Frame elements use a general 3-dimensional beam column formulation and it includes effects of biaxial bending, torsion, axial deformation and biaxial shear deformation. The slabs in the 3D structure are modeled as thin shell elements, which combine membrane and plate behavior and each joint in shell element has six degrees of freedom like the frame element. Hence the frame elements are directly connected to joints of shell elements and slabs are connected to beams and columns. The stiffness contributed by the walls to RC frames is an important factor to be taken into consideration in the modeling of a structure with infill walls. RC frames with unreinforced masonry walls are modelled as equivalent struts. Stiffness of struts depends on the width and thickness of the struts. Dimensions of struts were considered using the following expressions as mentioned in Eqs. (8)–(10) [31].

$$A_e = W_m t \tag{8}$$

$$W_m = 0.175 \times \alpha_h^{-0.4} \times L \tag{9}$$

$$\alpha_h = h \times \sqrt[4]{\frac{E_m t \sin(2\theta)}{4 E_f I_c h}} \tag{10}$$

Where,

E_m = Modulus of elasticity of unreinforced masonry infill (=645 MPa)

E_f = Modulus of elasticity of Moment Resisting Frame(MRF) (=28500 MPa)

I_c = Moment of inertia of the adjoining column.

θ = Angle of diagonal with horizontal (=36.3°).

A_e = Area of strut

W_m = the width of equivalent strut

t = the thickness of the infill wall (=0.23 m)

L = the length of the infill diagonal (=4.5 m)

h = floor to floor height of the building. (=3.3 m)

The width of the strut, W_m is obtained from the above equations as 0.45 m. For free vibration analysis, the base isolator is modelled as a linear spring with effective isolator stiffness of 7.1 kN/mm (initial stiffness of isolator is obtained from Fig. 5). For free vibration analysis both the building models are fixed at the base. The mode shapes of the two structures are shown in Fig. 7(a) and (b). Free vibration analysis of each of models was performed and the fundamental frequencies are tabulated in Table 3. It is observed from the table that, 1st mode frequency of the conventional building is 5.72 Hz and 4.82 Hz for longitudinal and transverse direction with mass participation of 72% and 78%, respectively. The 2nd mode frequency of the conventional building is 14.74 Hz and 13.83 Hz for longitudinal and transverse direction with mass participation of 24% and 19%, respectively. Fig. 7(a) shows the first fundamental mode of conventional building and Fig. 7(b) shows the first fundamental mode of base isolated building. In case of the base isolated building, 1st mode frequency of the structure is observed at 1.9 Hz and 1.85 Hz for longitudinal and transverse direction respectively with mass participation of 93%. Other mode of the base isolated building is 8.4 Hz and 7.8 Hz for longitudinal and transverse direction with approximately 2% mass participation. Thus, the frequency of base isolated structure is obtained as 1.9 Hz. However, the isolator was initially to be designed for 50 tons load on each isolator with the target design value of isolator frequency of 0.6 Hz. Hence, the post yield stiffness of each isolator considered initially for design was K_2 = 0.71 kN/mm (assuming full yielding of the isolator). However, after the design of the isolator, the post yield stiffness of the isolator, K_2 was obtained experimentally and theoretically as 0.82 kN/mm. Thus, considering this post yield stiffness and 50 tons load on each isolator, the design frequency of the isolator at which it will perform at its best is 0.64 Hz. But in reality, as the building is subjected to low acceleration, the yielding of isolator does not take place and the stiffness at which the isolator deforms is the initial stiffness, K_1 which is calculated as 7.1 kN/mm. Moreover, the total seismic mass of the superstructure (considering RC elements, brick walls and Superimposed dead load) on four base isolators is 180 Tons. Hence each of the four isolators is loaded with a mass of approximately 45 tons. The frequency of base isolated building is thus obtained as 1.85 Hz to 1.9 Hz instead of the design frequency of 0.64 Hz.

It is also observed from the Table 3 that base isolated structure has higher mode frequencies of 8.4 Hz and 7.8 Hz in longitudinal and transverse directions respectively. In low level of ground motion, the high initial stiffness of the isolation system excites higher modes in base-isolated structure and generates floor accelerations and story drift. Such behavior of the base-isolated building can be detrimental to sensitive equipment installed in the building especially if the equipment frequency matches with the frequency of the higher modes. This phenomenon was also reported by Sharma and Jangid [38].

6. Measured real earthquake response of the buildings

Response of the twin structures subjected to real earthquake are reported here. During the two earthquake events which occurred in 6th Nov., 2006 and 29th Nov., 2007 respectively, base isolated building response and the conventional structure response were measured. All

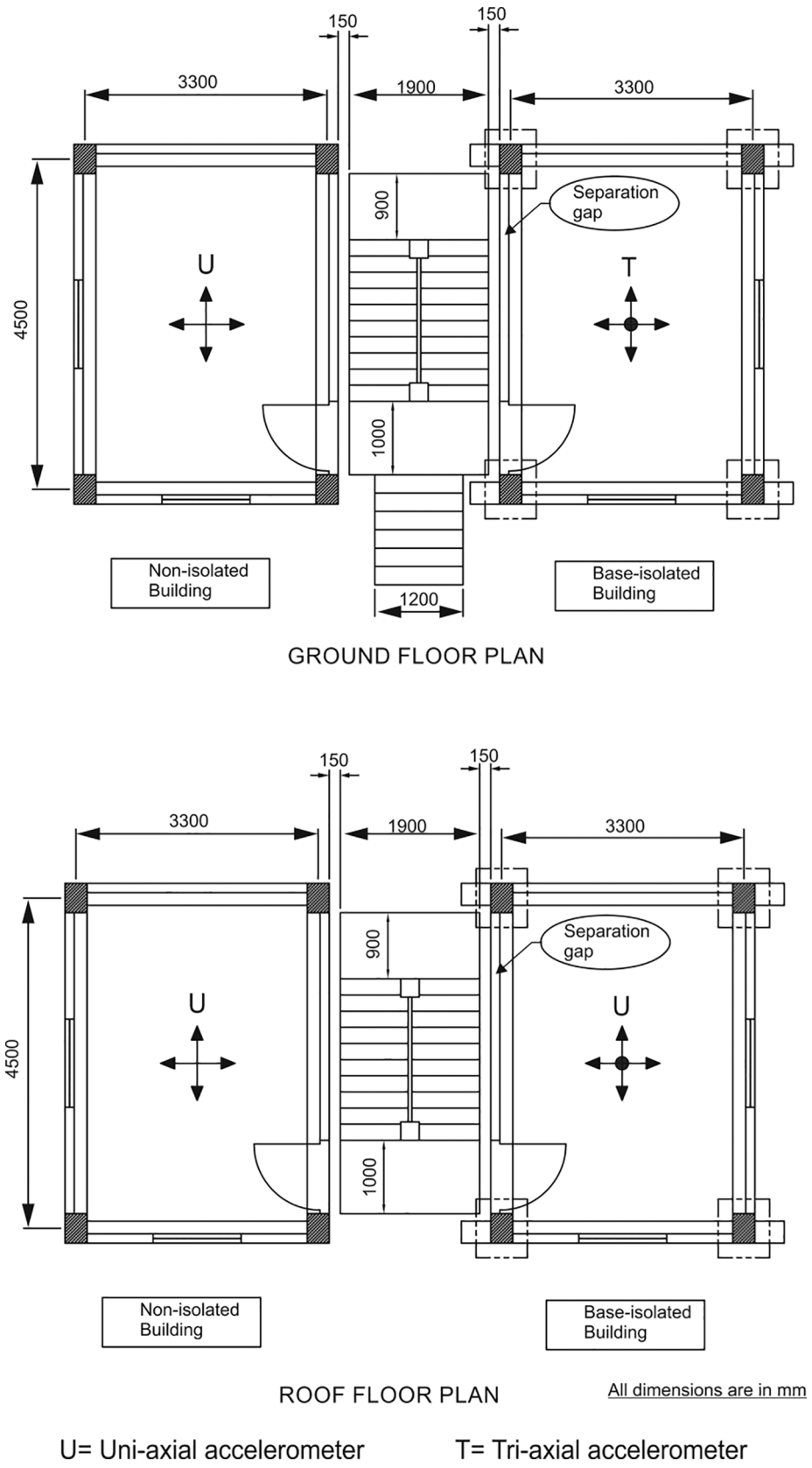

Fig. 6. Position of accelerometers in the prototype conventional and base isolated buildings at ground floor level and Roof level.

Table 2
: Instrumentation Details-Location, Channel Configuration and Nomenclature.

Channel No.	Description	Assigned Index
1	Instrument in Isolated Building recording acceleration in **Lon**gitudinal direction, on **R**oof level	ISO-LON-R
2	Instrument in **Iso**lated Building recording acceleration in **Tra**nsverse direction, on **R**oof level	ISO-TRA-R
3	Instrument in **Con**ventional Building recording acceleration in **Lon**gitudinal direction, on **R**oof level	CON-LON-R
4	Instrument in **Iso**lated Building recording acceleration in **Lon**gitudinal direction, on **F**irst floor level	ISO-LON-F
5	Instrument in **Iso**lated Building recording acceleration in **Tra**nsverse direction, on **F**irst floor level	ISO-TRA-F
6	Instrument in **Iso**lated Building recording acceleration in **Ver**tical direction, on **F**irst floor level	ISO-VER-F
7	Instrument under Conventional Building at **Gr**ound level recording **n**ear-**f**ield acceleration in **Lon**gitudinal direction	GRNF-LON
8	Instrument under Conventional Building at **Gr**ound level recording **n**ear-**f**ield acceleration in **Tra**nsverse direction	GRNF-TRA
9	Instrument under Conventional Building at **Gr**ound level recording **n**ear-**f**ield acceleration in **Ver**tical direction	GRNF-VER
10	Instrument in **Con**ventional Building recording acceleration in **Tra**nsverse direction, on **F**irst floor level	CON-TRA-F
11	Instrument in **Con**ventional Building recording acceleration in **Lon**gitudinal direction, on **F**irst floor level	CON-LON-F
12	Instrument in **Con**ventional Building recording acceleration in **Tra**nsverse direction, on **R**oof level	CON-TRA-R
Additional records at the site at free field		
1	Instrument located elsewhere in Guwahati at **Gr**ound level recording **f**ree-**f**ield acceleration in **Lon**gitudinal direction	GRFF-LON
2	Instrument located elsewhere in Guwahati at **Gr**ound level recording **f**ree-**f**ield acceleration in **Tra**nsverse direction	GRFF-TRA
3	Instrument located elsewhere in Guwahati at **Gr**ound level recording **f**ree-**f**ield acceleration in **Ver**tical direction	GRFF-VER

the reponse spectra generated in this paper are for 5% damping. Fig. 8 (a)–(d) shows the time history and response spectra of the free field motion in both the longitudinal and transverse directions for 6th Nov., 2006 earthquake measured at far field location for 5% damping. The longitudinal direction results are represented as solid line and transverse direction motions is represnted as dotted line. Fig. 8(e)–(h) shows the time history and response spectra of the motion below the conventional building in longitudinal and transverse directions for the 6th Nov., 2006 earthquake for 5% damping. Fig. 8(b) and (f) are the earthquake ground response spectra of same earthquake recorded in two different locations, one is away from the building and other one is just below the building respectively. A significant change in spectral shape is observed in the motion recorded below the building compared to the motion recorded away the from the building. Scattering, reflection and refraction of the wave from the nearby footing might be the reason of alteration of motion below the building. The dominent frequency content of the free field motion for earthquake dated 6th Nov., 2006 is 7 Hz to 10 Hz in longitudinal direction of the structure and 6 Hz to 12 Hz in transverse direction of the structure, while the dominent frequency content of the motion just below the buildings is 5.1 Hz, 8.9 Hz and 30 Hz in longitudinal direction and 4.2 Hz, 8.5 Hz, 14 Hz and 30 Hz in transverse direction. In Fig. 8(f) and (h) conventional building frequency is reported in response spectra of longitudinal and transverse direction of motion in the base motion in soil below the structures. Nevertheless, more amplification at the frequency of the conventional structure (4.19 Hz) is observed in the near field ground spectra of transverse direction than in the longitudinal direction. Thus, the base strata soil frequencies are shifted to 5.1 Hz and 4.19 Hz for the response measured below the buildings (from Fig. 8(f) and Fig. 8(h)). Here, the adjacent buildings show interaction through the common soil media. The interaction may have occured as there is change in motion due the presence of structure, which can be explained as a result of kinematic soil structure interaction. Also, in Fig. 8(f) and Fig. 8(h) two seperate spectral peaks are observed at 8.9 Hz and 8.5 Hz respectively. It shows that vibration energy is transferred from the structure to the soil and response of the soil is altered due the presence of the structure.

Fig. 9(a) and (b) shows the Floor Response Spectra (FRS) of the ground floor level and roof level for the conventional building for 5% damping. It is observed that the first fundamental frequencies of the building are 5.1 Hz and 4.2 Hz in longitudinal and transverse direction, respectively with soil structure interaction. The second peak in the FRS of ground floor as seen in Fig. 9(a) is at the second frequency of the structure which is 14.05 Hz in the transverse direction. This observation is in agreement with that made by Kothari et al. [39] which states that the peak of FRS at second frequency of the structure is higher at the ground floor of the structure than the roof level of the structure. Amplification of the peak floor acceleration at roof level with respect to the ground floor level is observed to be two times. The amplification of roof with respect to near field ground motion is 3.3 in longitudunal direction and 3.8 in transverse direction. Peak value of roof acceleration for conventional building at roof level is 0.01 g and 0.0076 g in transverse and longitudinal direction, respectively. Fig. 9(c) and (d) shows the response of the ground floor and roof level for longitudinal motion and tranverse motion, respectively in case of the base isolated building for 5% damping. From the figures it is noticed that building frequency with base isolator is 1.23 Hz, and a high peaks at 7.5 Hz and 9 Hz frequencies are observed in transverse and longitudinal directions respectively which are the second structural modes of the base isolated structure as per Table 3. This is because though the structure is placed on base isolators initial high stiffness of the isolators generates higher modes and as per Table 3, the second structural vibration mode occurs with 2% mass participation at 7.4 Hz and 8.5 Hz in transverse and longitudinal directions respectively. Thus, the superstructure modes of vibration observed in base isolated structure are due to initial stiffness of the isolator with first mode of 1.2 Hz and second mode of 7.5 Hz and 9 Hz in transverse and longitudinal directions. No amplification of the motion is observed in roof level with respect to the ground floor level in the base isolated building. Peak value of roof acceleration for base isolated building is observed as 0.0018 in both the directions which gives a reduction of 5.55 and 4.2 times in transverse and longitudinal directions, respectively with respect to conventional structure. In the FRS of the base isolated building, response frequencies of conventional structure are observed with a small peak at 4–5 Hz frequency. This due to the effect of nearby structure, observed in floor response spectra of base isolated building. The frequency of stiffer structure is observed in the adjacent flexible structure however, frequency of flexible structure is not observed in the response of stiffer structure.

Fig. 10(a)–(d) shows the time history and response spectra of the free field motion in both the longitudinal and transverse directions for earthquake dated 29th Nov., 2007, measured at far field location for 5% damping. Fig. 10(e)–(h) shows the motion recorded below the conventional building. Fig. 10(b) and (f) shows the response spectra of measured earthquake time histories, which were recorded away from the building and just below the building, respectively for 5% damping. The dominant frequency content of the free field motion for 2007 earthquake varies from 8 Hz to 15 Hz in longitudinal direction of the structure and 9 Hz to 15 Hz in transverse direction of the structure, while the dominant frequency content of the motion just below the buildings is 5.1 Hz, 15.9 Hz and 30 Hz in longitudinal direction and 4.2 Hz , 13.1 Hz and 30 Hz in transverse direction. Similar to the observation made during 2006 earthquake, the 2007 earthquake spectrum recorded just below the building has response peaks of nearby conventional building frequency. A peak 5.1 Hz peak is observed in Fig. 10(f) and a 4.2 Hz peak

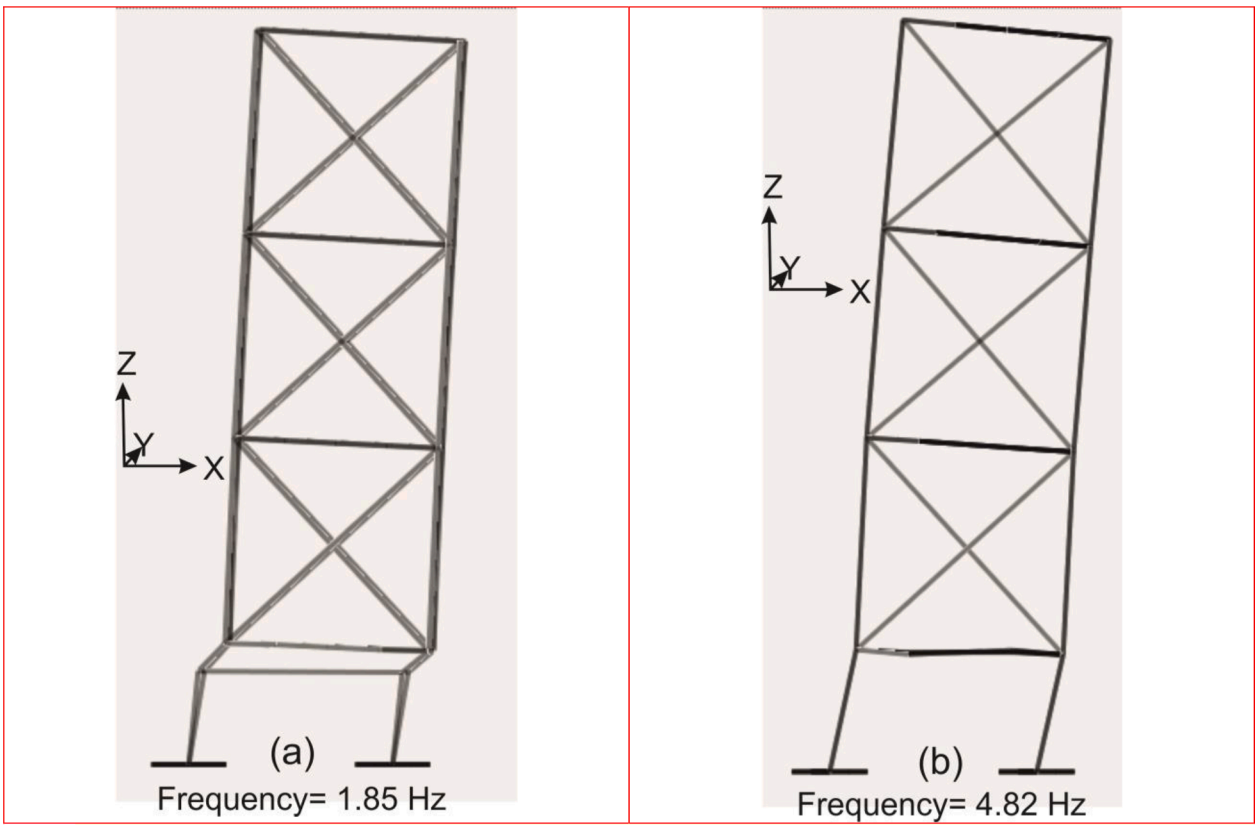

Fig. 7. Deformed mode shapes of buildings. (a) 1st mode shape of base isolator building building (Transverse direction), (b) 1st mode shape of conventional building building (Transverse direction).

Table 3
Frequency and Mass participation of both the structures.

Base Isolated structure		
Direction	Frequency	Mass participation %
Longitudinal	1.9 Hz	93
	8.4 Hz	2
Transverse	1.85 Hz	93
	7.8 Hz	2
Conventional structure- Fixed Base.		
Direction	Frequency	Mass participation %
Longitudinal	5.72 Hz	72
	14.74 Hz	24
Transverse	4.82 HZ	78
	13.83 Hz	19

is observed in Fig. 10(h) for longitudinal and transverse direction motion, respectively. Moreover, it is observed from Fig. 10(f) that PGA of the motion below the building was 0.0036 g which is same as far field while from Fig. 10(h), it is observed that PGA below the building is increased to 0.005 g at near field from 0.0036 g at far field . Presence of the nearby structure and scattering reflected wave from the nearby footing could be the possible cause of increased PGA and different frequency content in the near field response. Similar phenomenon was observed for the earthquake dated 6th Nov.,2006. Fig. 11 shows the Floor Response Spectra of the recorded 2007 earthquake at different floor levels of buildings for 5% damping. Fig. 11(a) and (b) shows the response of conventional building at ground floor and roof level response in both the directions, respectively. Amplification of 1.6 times is observed in peak floor acceleration of roof level with respect to ground floor level. Acceleration is amplified from 0.0036 g to 0.0057 g from ground floor level to roof floor level in longitudinal direction and for transverse direction response it is amplified to 0.008 g at roof level from 0.005 g at ground floor. From the figures, it is noticed that fundamental frequencies of conventional building are 5.2 Hz and 4.2 Hz in longitudinal direction and transverse direction, respectively. It is observed from FRS of the ground floor on conventional structure (Fig. 11(a)) that the second mode of the building is 18 Hz and 14 Hz for longitudinal and transverse direction respectively. Fig. 11(c) and (d) shows the response of the base isolated building for ground floor and roof location. In longitudinal and transverse directions no amplification was observed from ground floor level response to roof level response. Both the cases, PGA value is 0.0012 g and 0.0018 g for longitudinal direction and transverse direction respectively. Peak value of roof acceleration of base isolated structure shows a reduction of 4.44 and 4.75 times in transverse and longitudinal directions, respectively with respect to conventional structure. Influence of nearby structure in floor response spectra is also observed in Fig. 11(c) and (d). A peak in spectra is observed at 4.1 Hz and 5.15 Hz in response spectra of transverse and longitudinal direction respectively in base isolated building, which are the frequencies of nearby conventional building. In the base isolated structure, high peaks at 7.5 Hz and 9 Hz frequencies in transverse and longitudinal directions, respectively are observed which are which are the second structural modes of the base isolated structure as per Table 3 similar to the previous earthquake (2006) case.

From the above discussion it is observed that for both the real earthquakes, response of the base isolated building has been reduced due to lead rubber bearing. Nearly 4 to 5 times reduction of the roof acceleration for base isolated building is observed as compared to conventional building for both the earthquakes. Also frequencies of rigid conventional structure of 4.2 Hz and 5.1 Hz (in transverse and longitudinal directions respectively) are observed in response of flexible base isolated structure due to Structure Soil Structure Interaction (SSSI).

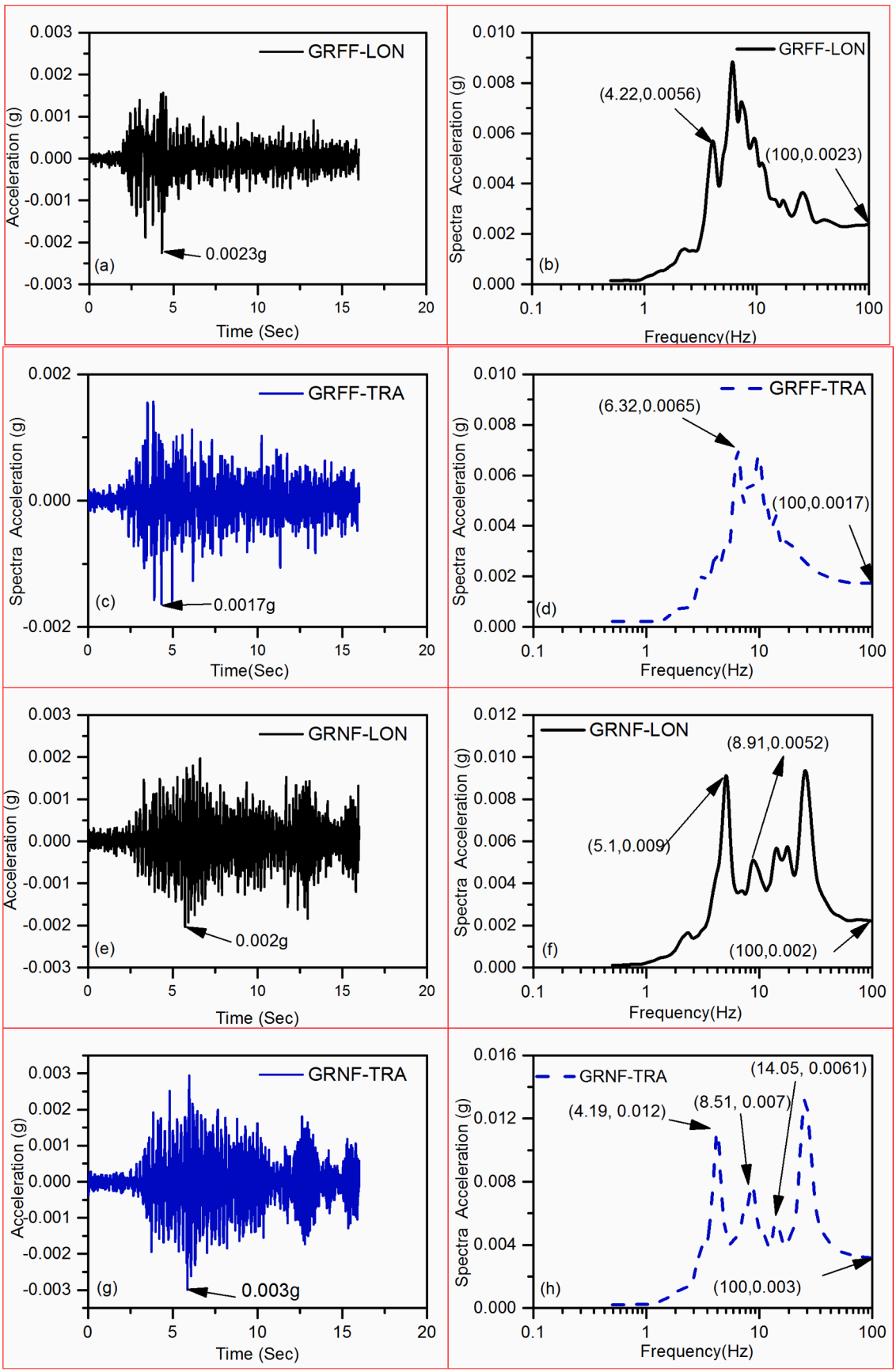

Fig. 8. Longitudinal and transverse direction earthquake motion and corresponding response spectra recorded on ground surface of earthquake dated 06/11/2006. (a)–(d) Earthquake motion recorded away from the building and (e)-(h) Earthquake motion recorded just below the conventional building.

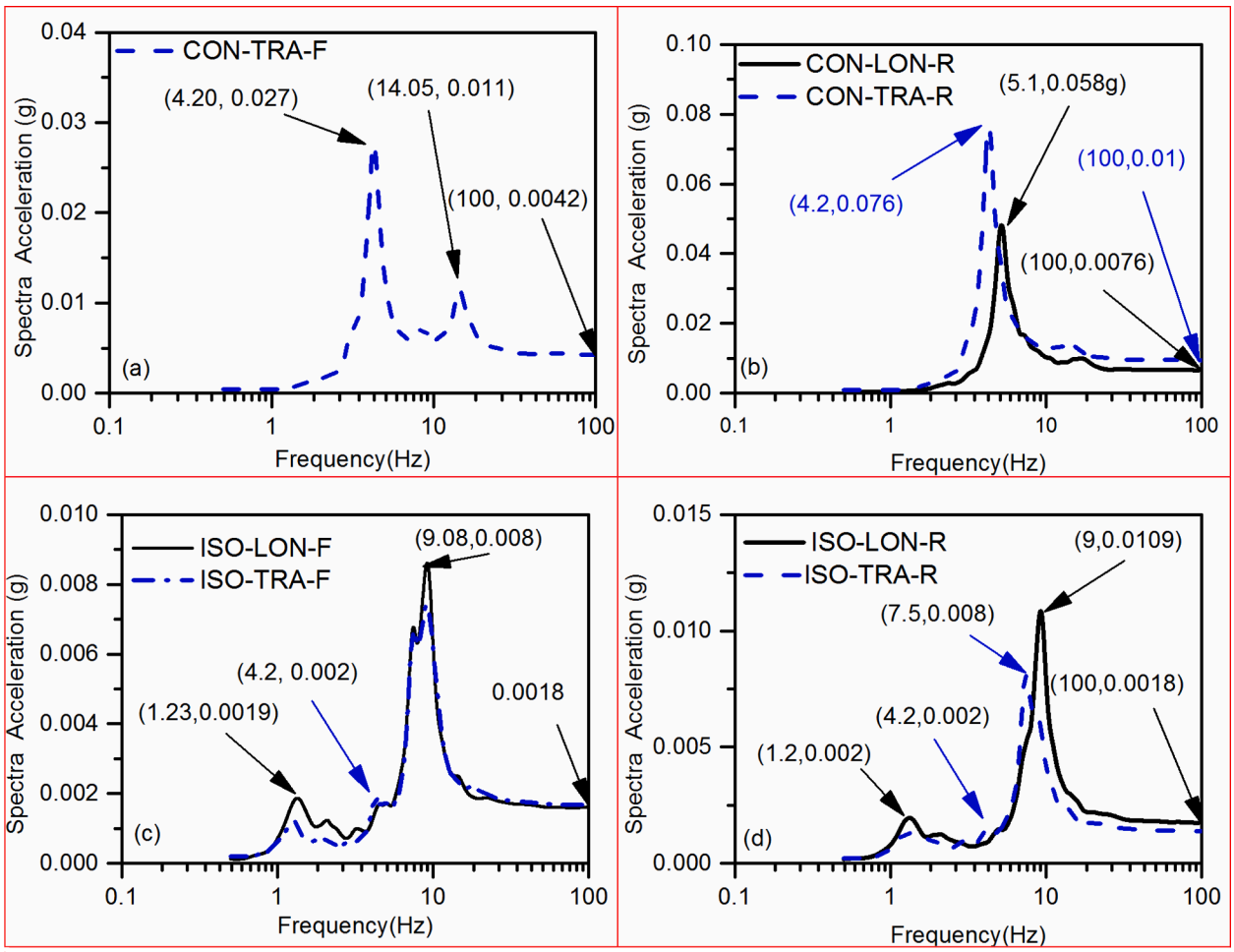

Fig. 9. Longitudinal and transverse direction building response and corresponding response spectra recorded on various floor level of earthquake dated 06/11/2006. (a)–(b) Earthquake motion recorded at ground floor ad roof level of conventional building. (c)-(d) Earthquake motion recorded at ground floor and roof level of base isolated building (5% damping).

7. Numerical modelling

In this section, an attempt is made to simulate the complex soil structure interaction of the two structures with soil using numerical modelling. Finite Element software, MIDAS GTS/NX [36] is used for modelling and analysis. Nonlinear time history analysis module has been used to simulate dynamic response of twin structure along with soil domain. Size of each one single building is 4.5 m × 3.3 m and gap between two building is 2.2 m. A soil domain of area 100 m × 100 m and depth of 30 m is considered. Boundaries are kept far from the foundation of the building to minimize the boundary effects. In this study, all beams and columns are modeled as beam element, and soil is modeled as 8 nodded brick elements with three translational degrees freedom per node. Shell elements are used to model the floor slab and foundation of the structure and footing. The shell element has four nodes and each node has 6 degrees of freedom. Six degrees of freedom include three rotational degree of freedom and three translational degree of freedom. Building foundation is embedded into the soil element. Details of numerical modeling is shown in Fig. 12. Buildings are made of reinforced concrete with M30 grade of concrete having strength 30 N/mm^2. Density of the concrete is 2500 kg/m^3 and Young's modulus of the concrete is 27.3 GPa [40]. Soil properties plays an important role in soil structure interaction. During cyclic loading the stress–strain behavior of soil is non-linear and even for very small shear strains (less than 0.001% [41]) soil exhibit hysteretic behavior. Material properties and dynamic characteristics of soil were not measured at study area, so dynamic property of the soil (such as shear modulus of soil) is obtained from the shear wave velocity profile of the nearby location. The distribution of the profile of shear wave velocity with depth as shown in Fig. 2, is considered for modeling the soil in three layers viz. of 5 m, 8 m, and 17 m thickness each with shear wave velocity, V_s of 120 m/s, 250 m/s and 350 m/s respectively. The site was located near the Brahmaputra river bank. Representative soil properties for Brahmaputra sand (BS) is collected from Kumar et al. [42] and were used in the analysis. Shear modulus degradation curve with shear strain of soil is reported in Fig. 13. Small strain shear modulus of soil, G_{max} is obtained from Shear wave velocity, V_s and density, ρ using Eq. (11).

$$G_{max} = \rho V_s^2 \tag{11}$$

In order to develop constitutive stress strain relationship under cyclic loading hysterisis loops are often constructed using a backbone curve. In recent days, for simulation of dynamic behavior of soil various advanced nonlinear soil plasticity models are available in literature and these require various soil parameters. Due to lack of proper soil cyclic test results, simplified Modified Ramberg-Osgood (R-O) model is used to simulate the nonlinear behavior of soil subjected to dynamic loading. The R-O parameters generally fit backbone curves and modulus-strain data quite well at shearing strains less than 0.1%. Modified Ramberg-Osgood (M−R−O) model is available in MIDAS GTS/NX material library module. M−R−O model is used to implement nonlinear shear degradation curve [43]. One form of the Ramberg-Osgood stress–strain equation for the backbone curve can be written as follows

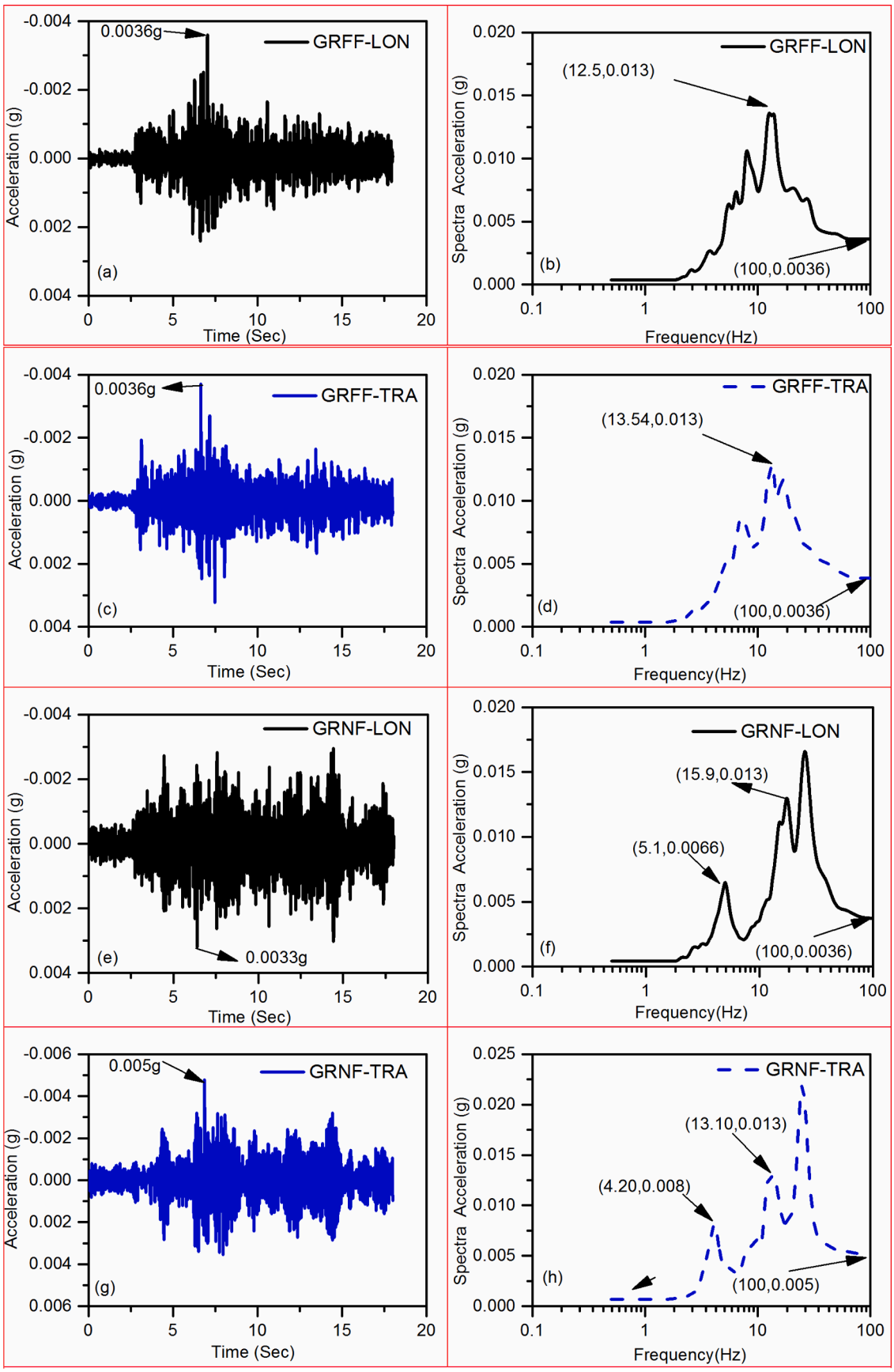

Fig. 10. Longitudinal and transverse direction earthquake motion and corresponding response spectra recorded on ground surface of earthquake dated 29/11/2007. (a)–(d) Earthquake motion recorded at away from the building and (e)–(h) Earthquake motion recorded just below the conventional building.

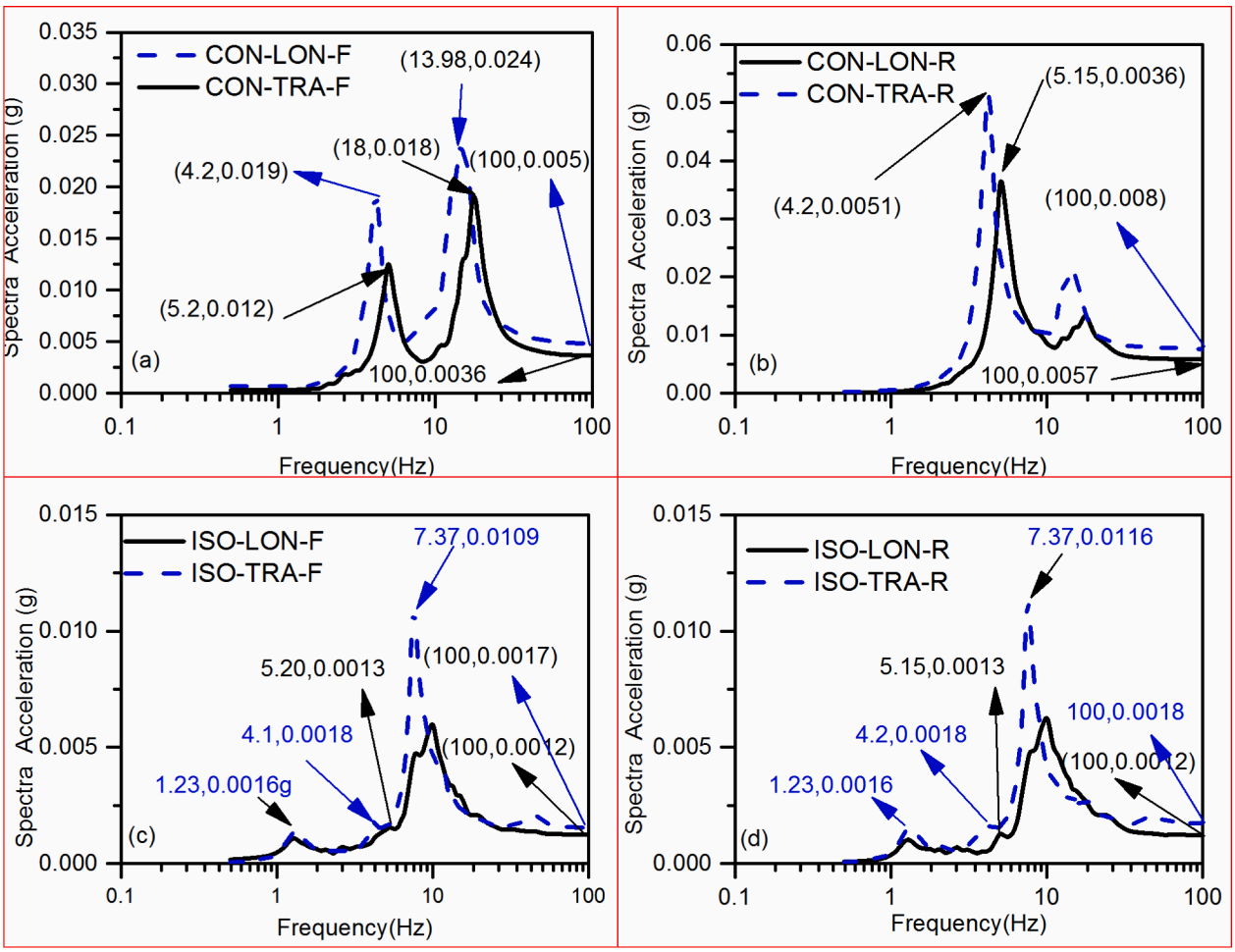

Fig. 11. Longitudinal and transverse direction building response and corresponding response spectra recorded on various floor level of earthquake dated 29/11/2007. (a),(b) Earthquake motion recorded at ground floor ad roof level of conventional building. (c)-(d) Earthquake motion recorded at ground floor ad roof level of base isolated building (5% Damping).

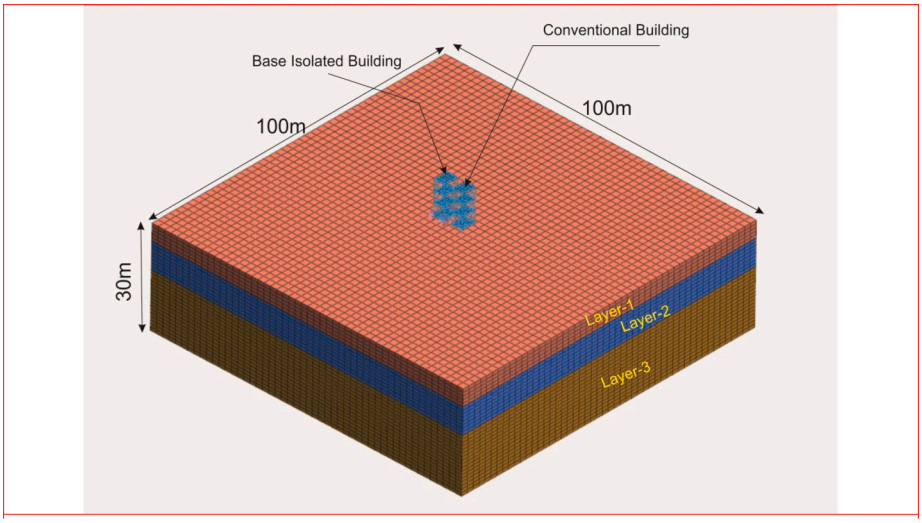

Fig. 12. Finite element mesh of numerical modeling.

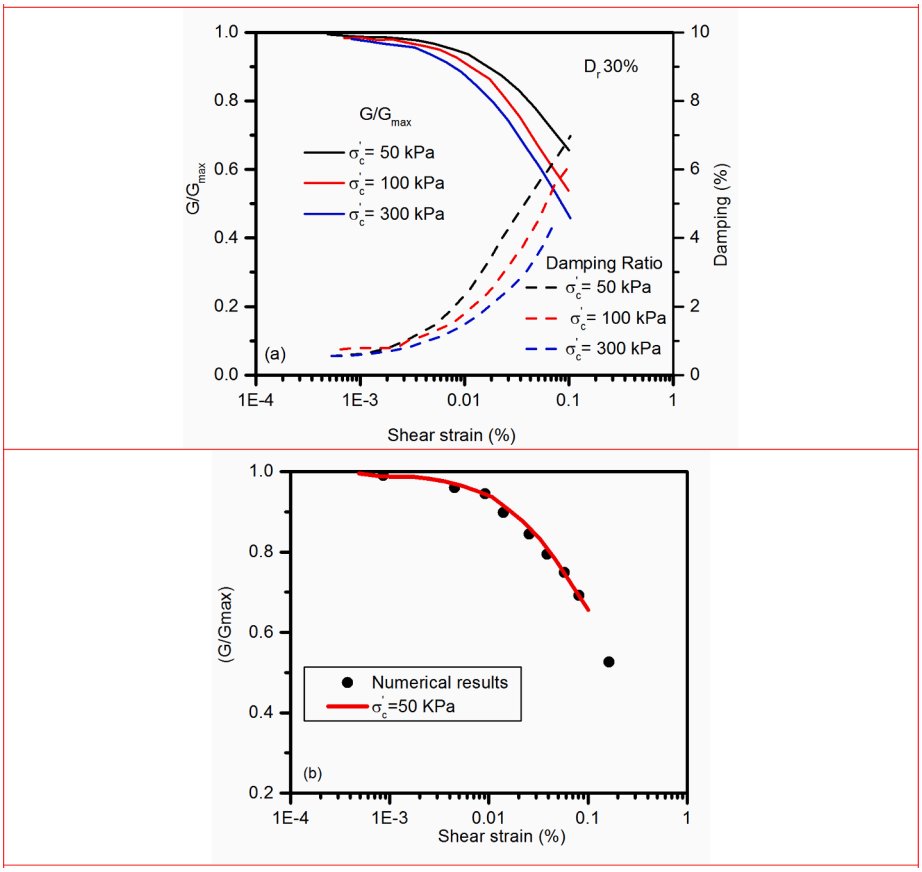

Fig. 13. (a) Dynamic properties of Brahmaputra Sand (BS). [42] (b) Single element validation of numerical model.

$$G_{max}\gamma = \tau + \alpha|\tau|^{\beta}\tau \tag{12}$$

$$\beta = \frac{2\pi h_{max}}{2 - \pi h_{max}} \tag{13}$$

$$\alpha = \left(\frac{2}{\gamma_r G_{max}}\right)^{\beta} \tag{14}$$

Where, G_{max} is initial shear modulus, γ_r is the reference strain, h_{max} is the maximum damping and γ, τ are shear strain and stress respectively.

For unloading and reloading of hysteresis curve is as follows

$$G_{max}\left(\frac{\gamma \pm \gamma_1}{2}\right) = \left(\frac{\tau \pm \tau_1}{2}\right)\left(1 + \alpha\left(\tau\frac{\tau \pm \tau_1}{2}\right)^{\beta}\right) \tag{15}$$

In (15) γ_1 and τ_1 are the shear strain and stress values at the load reversal point. Small strain shear modulus varies between 30 MPa at surface to 245 MPa at the 30 m below, which correspond to the shear wave velocity of 120 m/s and 350 m/s, respectively. Apart from the small strain shear modulus of the the soil, reference strain of the soil is also a required parameter which will control the shear modulus degradation curve. Details of soil parameters are given in Table 4. Behavior of soil model subjected to dynamic loading, obtained from experiments performed by Dammala et.al. [42] is verified with numerical simulation of a single element. A 1 m × 1 m × 1 m single soil element is modeled and sinusoidal force of varying amplitude is applied. For each analysis shear strain and shear modulus degradation are obtained and results are verified with the target (experimental) shear modulus and shear strain degradation curve. Fig. 13(b) shows a good agreement between numerical results and target curve. The maximum element size should satisfy the requirement of ASCE 4–16 [44], otherwise high frequency content can not be simulated accurately. The requirement is given below.

Table 4
Soil parameters used in the analysis.

Soil layer	Thickness	Average Vs (m/s)	Density (kg/m^3)	Initial shear modulus	Reference strain
Layer-1	5	120	1800	30,420	0.0035
Layer-2	8	250	1800	112,500	0.0049
Layer-3	17	350	2000	245,000	0.0043

$$l_{ele} \leqslant \frac{V_s}{N.f_{max}} \tag{16}$$

Where, l_{ele} is vertical size of the element, and V_s is shear wave velocity of the layer, f_{max} is the cutoff frequency of the analysis an N is constant (generally > 4). In this study, the maximum element size is calculated from the smallest small strain shear wave velocity divided by 8 times the maximum frequency of the interest. Here, the maximum frequency of interest is 20 Hz, which is more than the 2nd fundamental frequency of the conventional building structure. Hence maximum element size is obtained as 1 m. In order to avoid reflection of wave from the boundary, free field elements are implemented at the boundary. Seismic motion measured away from the buildings is considered as free surface motion (motion GRFF-LON and GRFF-TRA). The free surface motion is de-convoluted and motion at 30 m below the ground level is obtained using DEEPSOIL software [45]. The motion obtained after deconvolution is applied at the end of soil layer of numerical model in longitudinal and transverse directions. Similar methodology was adopted by Rayani et al.[46]. In the present numerical study, earthquake recorded on 29th Nov., 2007 is used. Details of ground motion are explained in Fig. 10(a)–(d). Main objective of the study is to simulate the

structure soil structure interaction. Some assumptions are made to simplify the simulation environment in terms of base isolator modelling and make the simulated motion more appropriate. In nonlinear time history analysis, base isolator is simulated with a beam element with bilinear hinge properties. Responses are measured at ground floor level and roof level for both the buildings.

8. Comparision of numerical results

Results obtained from the numerical studies are compared with the data observed from real earthquakes. For comparison purpose, only building responses are considered and reported in Fig. 14. Fig. 14(a)–(d) shows the comparision between real earthquake response of the base isolated building with the response obtained from the numerical analysis of the base isolated building for 5% damping. It is observed that numerical results predicted well with the recorded earthquake in terms of major frequencies. For the base isolated structure, numerical analysis shows two frequencies. The first frequency is the isolator frequency which is 1.9 Hz. The second frequency is structural frequency as explained in the preceding section and with soil modeling, this frequency is obtained numerically as 8.4 Hz and 7.8 Hz in longitudinal and transverse directions respectively. Peak floor acceleration response at ground floor level and roof level is predicted well for the transverse and longitudinal directions motion as 0.0018 g and 0.0012 g respectively. First mode frequency of the base isolated building is predicted higher than the actual value, which may be due to modeling uncertainities in actual structure and soil. The flexibility of soil plays role in reducing the isolator frequency with soil , hence the fixed base isolator frequency of 1.9 Hz (as given in Table 3) is reduced to 1.23 Hz in actual measurement and it is reduced to 1.8 Hz in numerical simulation with the soil. Fig. 14 (e)-(h) shows the comparison of response spectra of the numerical prediction and recorded response for conventional building subjected to real earthquake dated 29th Nov., 2007. Here, it is observed that peak floor response and 1st mode of the building are predicted well with the recorded data, but for the second mode of the structure numerical results predict higher floor spectral acceleration values than the recorded floor response specttrum (FRS) values. The first and the second frequency of the structure observed from this numerical model considering soil is 5.05 Hz and 14.38 Hz in longitudinal direction and 4.74 Hz and 13.25 Hz in transverse direction. It was observed in the preceding section (see Table 3) that the fixed based first and second frequencies in longitudinal direction are 5.72 Hz and 14.74 Hz respectively and in transverse direction are 4.82 Hz and 13.83 Hz respectively. The value of fixed base frequencies are slightly higher than the frequencies obtained from numerical model with soil. This is due to soil flexibility present in the numerical model. It is observed that in reality the soil is more flexible than the numerical soil model as the actual frequency of the building with isolator and that of the conventional building are lesser than that obtained from numerical model with soil modeling. The uncertainity in the soil parameters may be the reason for this difference. Moreover, energy dissipation of the real structure is a complex phenomenon and that might not be exactly captured in numerical modleling due to few simplistic assumptions such as, brick wall being modelled as equivalent strut element. However, in numerical modelling structure soil structure interaction (SSSI) is observed for the base isolated structure. In Fig. 14 (b) and (d), a small frequency peak at 4.2 Hz is observed which corresponds to the frequency of nearby conventional building. As a whole, numerical results are in very good agreement with those measured during the real earthquake. The results capture most of the major phenomenon such as fundamental frequencies of structures, structure soil structure interaction and peak floor response acceleration.

9. Response of the building in site specific earthquake

The buildings are in reality subjected to very small levels of earthquakes for which the isolator does not yield . Hence a case study is performed in this section, by studying the building response for possible higher design basis earthquake loads. The study is performed by giving both the buildings an input acceleration of 0.26 g corresponding to site specific Response Spectrum PGA. For this purpose, same numerical modeling procedure is used and a site specific spectrum compatible target time history is appled as an input motion. Details of generation of site specific response spectra is explained in Das et al. [47]. Das et al. [47] performed an extensive study in North-East India and developed a new attenuation model based on pseudo-spectral velocity scaling function by using 261 recorded accelerograms in Northeast India. They also performed probabilistic seismic hazard analysis (PSHA) for North-East India with newly developed attenuation relationship. After performing PSHA, a Uniform Hazard Response Spectra (UHRS) was proposed for a return period of 100 years with 50% confidence level for horizontal component of ground motion at the Guwahati region. The peak ground acceleration (PGA) of this UHRS is 0.26 g. The target site specific response spectra for the Guwahati region for 5% damping is shown in Fig. 15. A site specific uniform hazard spectrum compatible time history is generated by SIMQKE [48] and is shown in Fig. 16. Baseline correction of the spectrum compatible time history is obtained using DEEPSOIL software [45]. Earthquake spectrum generated from the time history is compared with target spectrum for 5% damping and is shown in Fig. 15**.** Spectrum compatible time history is applied in both longitudinal and transverse directions to the numerical model and reponses of both the buildings are captured at roof level.

Fig. 17(a) and (b) shows the roof level floor response spectra of the base isolated building and the conventional building in longitudunal directon when subjected to site specific target ground motion. As shown in the Fig. 17(a) peak floor response at roof level of base isolated building is 0.18 g, and the peak roof level floor response of conventional building response is 0.73 g. 4.1 times reduction in floor acceleration response of base isolated building is observed compared to the conventional building subjected to the same earthquake. Fig. 17(a) shows that the base isolated building frequency shifts from 1.9 Hz corresponding to low level earthquake of PGA 0.002 g to 1.45 Hz for high level earthquake of PGA 0.26 g. Conventional building peak frequency of 4.8 Hz is also reflected in the response of base isolated building. It is also observed that the first fundamental frequency of conventional structure in longitudinal direction is reduced from 5.1 Hz corresponding to low level earthquake of PGA 0.002 g to 4.9 Hz for high level earthquake of PGA 0.26 g. This is due to the soil nonlinearity experienced in the numerical model at high excitation of 0.26 g PGA. It is also observed that floor spectra of roof of base isolated structure has multiple frequencies. This is due to nonlinear deformation of the isolator which gives different effective stiffness for different displacements in the hysteretic deformation of the isolator experienced during cyclic motion as shown in Fig. 18. Maximum displacement at isolator level is observed 12.53 mm. The maximum range of frequency considering the effetive stiffness is between 1.45 and 1.9 Hz for the isolator. Hence average frequency of 1.7 Hz can be assumed for the isolators considering all the hysteretic loops of the isolator. Fig. 19(a) and (b) show the roof level displacement time history of top floor of base isolated building and conventional building. Maximum of 13.97 mm displacement is noticed in top floor of base isolated building, whereas 8 mm displacement is observed in conventional building. Series of analysis is performed on the numerical model of base isolated building with soil for different scaled up PGA of target motion. It is noticed from the analysis that frequency of the base isolated building reduces with increasing peak ground acceleration. As the PGA increases from 0.002 g to 0.5 g, it is is observed that first mode frequency of the base isolator varies from 1.9 Hz to 1.3 Hz. Fig. 20 shows the variation of frequency of the base isolated building with PGA.

Roof level acceleration of conventional building is 0.73 g. At this high level of acceleration, brick walls of the conventional structure may fail. Hence, further nonlinear dynamic analysis of the numerical model is performed for 0.26 g PGA, considering conventional structure without

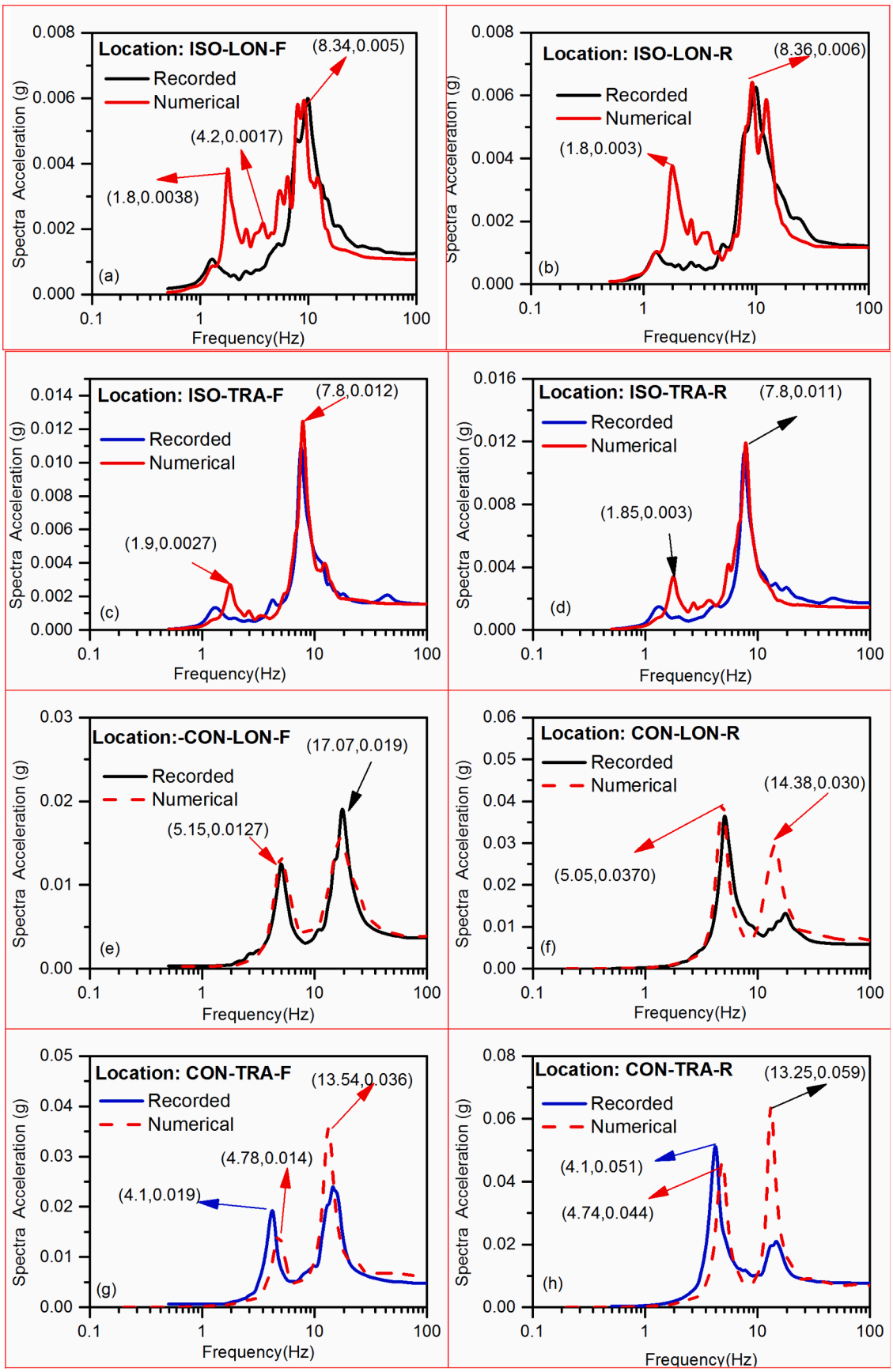

Fig. 14. Comparison of numerical results with recorded earthquake in different floor level of conventional building and isolated building.

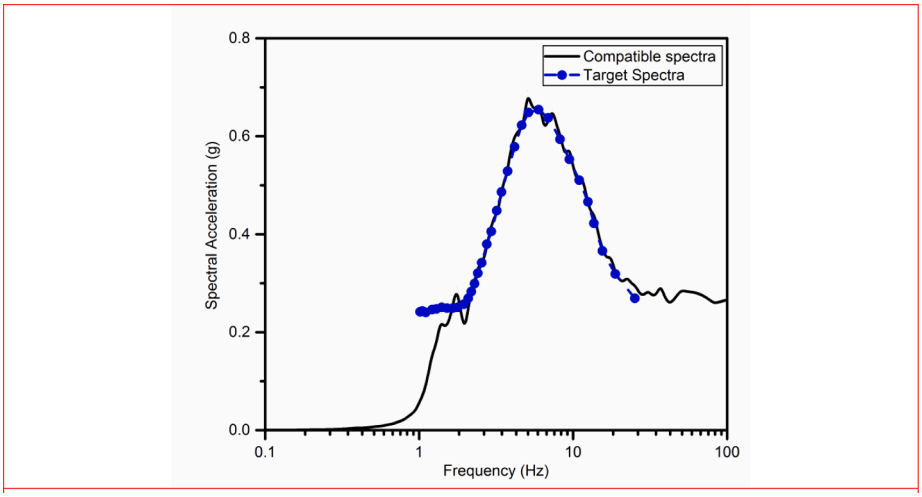

Fig. 15. Comparison of target spectra and spectrum compatible time history.

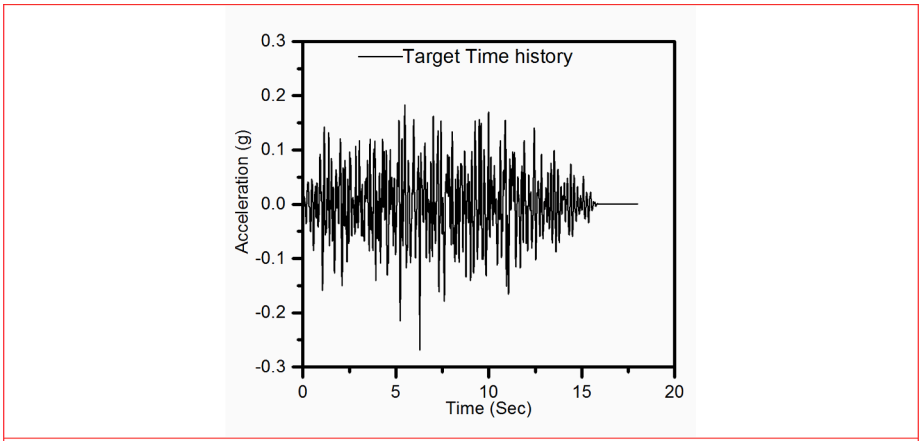

Fig. 16. Spectrum compatible timehistory.

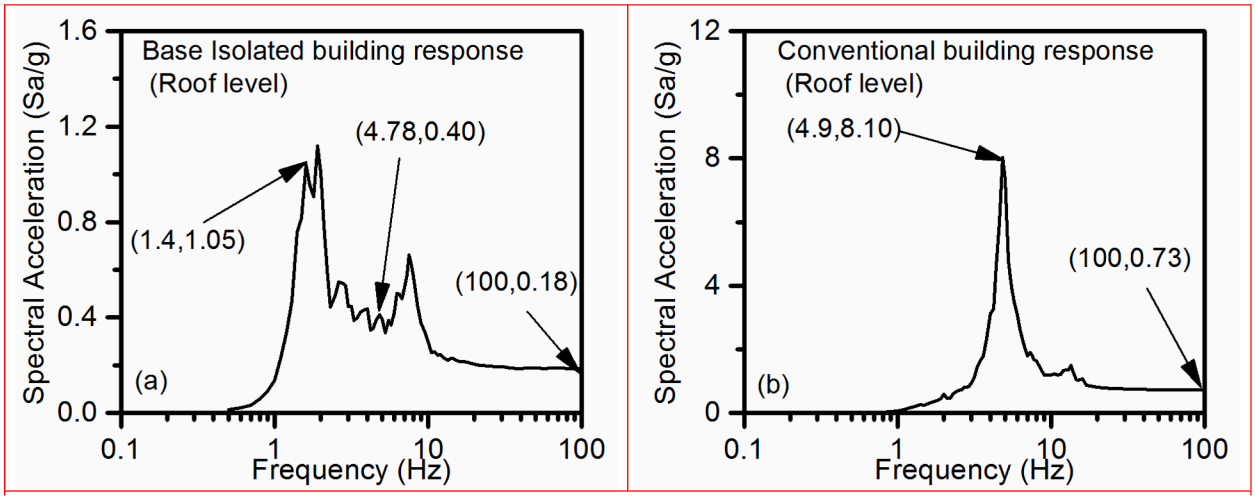

Fig. 17. (a) Roof level spectra of base isolated building subjected to target motion. (b) Roof level spectra of Conventional building subjected to target motion (5% damping).

wall stiffness and wall mass. Roof level floor response spectra and roof level floor displacement time history obtained from the numerical simulation are plotted in Fig. 21(a) and (b) respectively. From Fig. 21(a), it is noticed that building frequency reduced to 2.9 Hz from 4.9 Hz (considering wall stiffness) and roof level acceleration is reduced to 0.63 g from 0.73 g. In Fig. 21(b) it is also noticed that roof deformation is

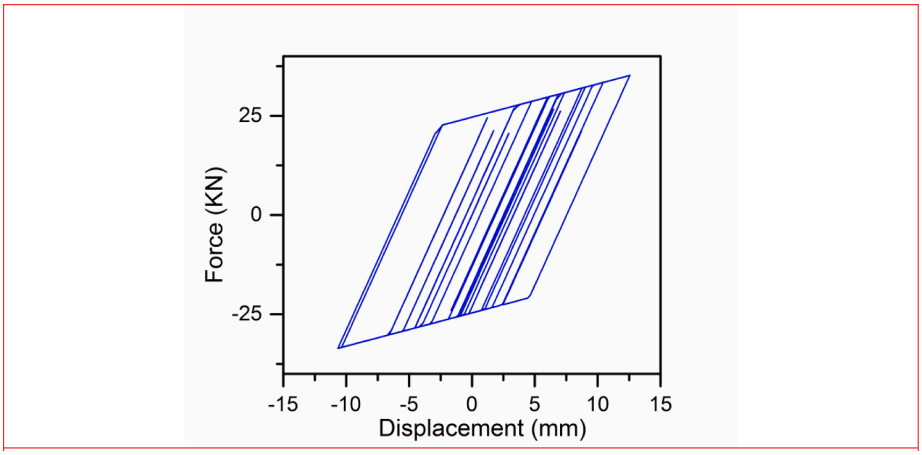

Fig. 18. Force displacement charecteristics of isolator (modeled as nonlinear link) subjected to target motion.

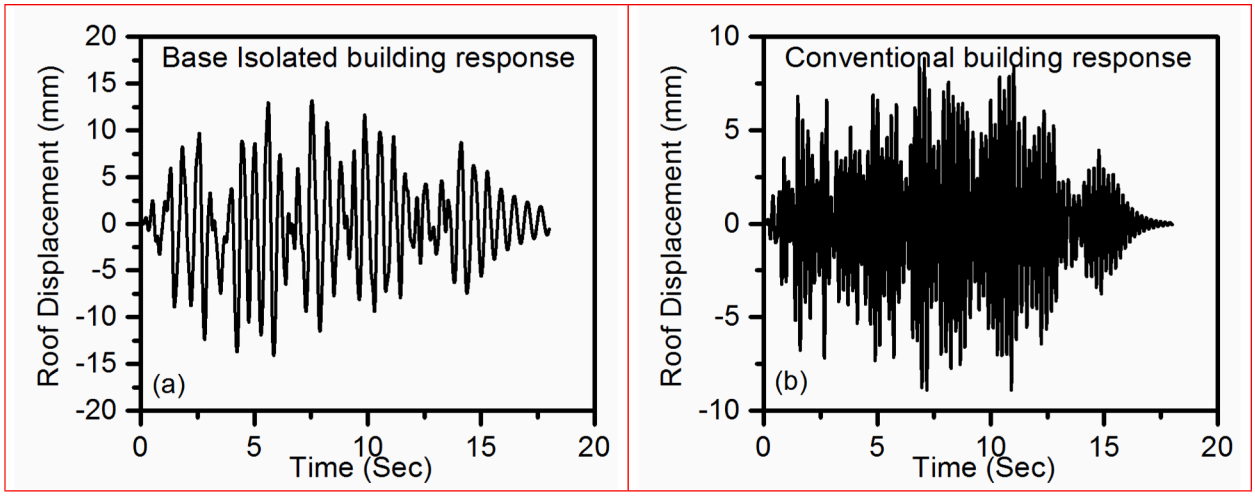

Fig. 19. (a) Roof level displacement of base isolated building subjected to target motion. (b) Roof level displacement of Conventional building subjected to target motion.

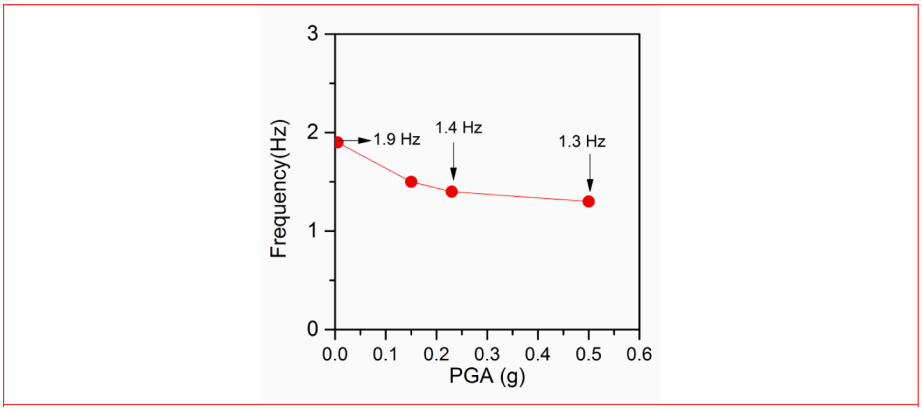

Fig. 20. Variation of 1st mode frequency of base-isolated structure with PGA.

increased with increasing flexibility of the structure. Here, for the structure without wall stiffness, 18 mm peak roof displacement is obtained compared to 8 mm peak roof displacement obtained considering wall stiffness.

10. Conclusion

In the present paper, seismic response of two RC framed structures, one mounted on base isolator (LRB) and other a conventional structure subjected to two real earthquakes (2006 and 2007) motions are studied. Numerical modeling of both the buildings is carried out by nonlinear

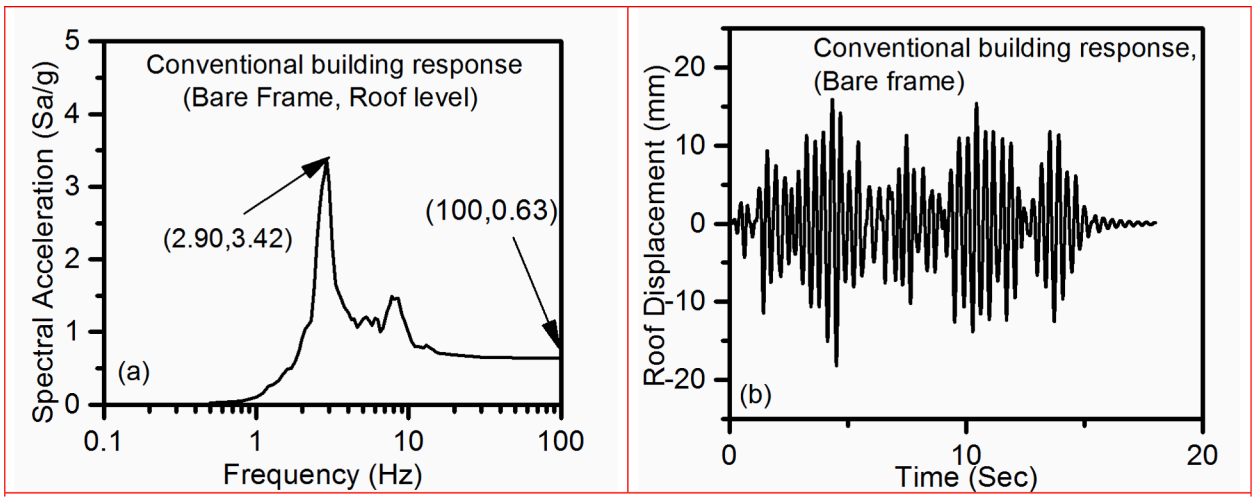

Fig. 21. (a) Roof level spectra of Conventional building subjected to target motion (Bare frame condition.) (b) Roof level displacement time history of Conventional building subjected to target motion.(Bare frame condition) (All the response spectrums are generated for 5% damping).

modeling of the soil strata and the isolators and the numerical responses are compared with recorded responses of the two earthquakes for both the structures. Moreover, responses of the same buildings are also obtained for site specific earthquake ground motion considering fully nonlinear behavior of soil and the isolators. The following conclusions are drawn from the results of numerical simulations and recorded response of the buildings.

1) The dominant frequency content of the free field motion for the real earthquake varies from 6 Hz to 15 Hz in both the horizontal directions, while the dominant frequency content of the motion just below the buildings show discrete frequencies between 4 and 5 Hz, 13 to 15 Hz and 30 Hz in both horizontal directions. Thus, the response spectrum recorded just below the building shows the response peaks of nearby conventional building frequencies. This is due to interaction of the adjacent buildings through kinematic soil structure interaction with common soil media.
2) The frequencies of the conventional structure with soil structure interaction in both the longitudinal and transverse horizontal directions are 5.1 Hz and 4.1 Hz, respectively. The design frequency of the building with isolator at which it will perform at its best with full hysteretic loop is 0.64 Hz. However, in reality, as the buildings are subjected to low level ground acceleration, full yielding of isolator is not experienced. Also, the actual building mass on the isolators is lesser than that at which it was designed so the frequency of the base isolated building was observed as 1.24 Hz from measurement and it was 1.85 Hz from numerical simulation. Base isolated structure has measured higher modes of 8.4 Hz and 7.8 Hz in horizontal longitudinal and transverse directions, respectively which are also captured in numerical simulation. These are due to high initial stiffness of the isolation system which excites higher modes in base-isolated structure and generates floor accelerations and story drift.
3) It is observed that response of the base isolated building is reduced by nearly 4 to 5 times at the roof level as compared to conventional building for both the earthquakes held in 2006 and 2007. However, in the FRS of the base isolated building, response frequencies of conventional structure are observed with a small peak at 4–5 Hz frequency. This is due to the effect of nearby structure and structure soil structure interaction. Thus the effect of adjacently located stiffer structure is observed in the response of the flexible structure. However, frequency of flexible structure is not observed in the response of stiffer structure.
4) The numerical simulation carried out with detailed soil structure interaction shows good agreement with the records obtained from the real earthquake with good match in the frequencies of the earthquake motion at each floor levels of both the structures. However, it is observed that the second peak of conventional structure in both the roof and first floor FRS is higher in numerical simulation than actually recorded one. In case of base isolated structure, the first peak in both the roof and first floor FRS is higher in numerical simulation than actually recorded one. This is due to local vibration modes of the elements of the structure coinciding with the global modes of the structure in numerical analysis which may not be there in actual structure. The modelling uncertainties like walls modelled as strut elements etc. may be one of the reasons for this discrepancy.
5) Numerical analysis carried out for higher earthquake shows distinctly different FRS for the base isolated structure than that for the very less magnitude earthquake. The FRS of the base isolated structure has multiple frequencies. This is due to nonlinear deformation of the isolator which gives different effective stiffness for different displacements in the hysteretic deformation of the isolator experienced during cyclic motion. It is observed that the FRS peaks of base isolated structure at certain frequencies have acceleration almost equal to FRS of conventional structure though the peak floor/roof acceleration of base isolated structure is 4.1 times lesser than that of the conventional structure for same ground motion. Such behavior of base isolated structure can be detrimental to sensitive equipment installed in the building especially if the equipment frequency matches with the frequency of the higher modes. In future, the acceleration sensitive and displacement sensitive secondary equipment will be placed on the structures and their response when subjected to real earthquakes will be measured. Moreover, their behaviour in the case of large earthquakes will be studied.

Declaration of Competing Interest

The authors declare that they have no known competing financial interests or personal relationships that could have appeared to influence the work reported in this paper.

Acknowledgments

The authors would like to thank four anonymous reviewers, whose comments/suggestions helped improve and clarify this manuscript.The authors would like to thank Prof. S. K. Deb of Civil engineering department, IIT Guwahati, and Shri P. N. Dubey from Bhabha Atomic Research Center, Mumbai, for sharing earthquake data and other model related information through Board of Research of Nuclear Sciences

(BRNS) project. Authors would also like to thank Prof Arindam Dey and his team of Civil engineering department, IIT Guwahati for sharing soil data of the study area.

References

[1] Kelly JM. Aseismic base isolation: review and bibliography. Soil Dyn Earthquake Eng 1986;5(4):202–16.
[2] Rahnavard R, Craveiro HD, Napolitano R. Static and dynamic stability analysis of a steel-rubber isolator with rubber cores. Structures: Elsevier; 2020. p. 441-55.
[3] Rahnavard R, Thomas RJ. Numerical evaluation of steel-rubber isolator with single and multiple rubber cores. Eng Struct 2019;198:109532. https://doi.org/10.1016/j.engstruct.2019.109532.
[4] Sheikhi J, Fathi M, Rahnavard R. Natural rubber bearing incorporated with high toughness steel ring dampers. Structures: Elsevier; 2020. p. 107-23.
[5] Tsai CS, Chiang T-C, Chen B-J. Shaking table tests of a full scale steel structure isolated with MFPS. ASME 2003 Pressure Vessels and Piping Conference. Am Soc Mech Eng Digital Collect 2003:41–7.
[6] Hu JW. Response of seismically isolated steel frame buildings with sustainable lead-rubber bearing (LRB) isolator devices subjected to near-fault (NF) ground motions. Sustainability 2015;7:111–37.
[7] Jangid RS. Optimum lead–rubber isolation bearings for near-fault motions. Eng Struct 2007;29(10):2503–13.
[8] Kelly JM, Hodder SB. Experimental study of lead and elastomeric dampers for base isolation systems. University of California. Earthquake Eng Res Center 1981.
[9] Hameed A, Koo M-S, Do TD, Jeong J-H. Effect of lead rubber bearing characteristics on the response of seismic-isolated bridges. KSCE J Civ Eng 2008;12(3):187–96.
[10] Nagarajaiah S, Xiaohong S. Response of base-isolated USC hospital building in Northridge earthquake. J Struct Eng 2000;126(10):1177–86.
[11] Ryan KL, Chopra AK. Estimation of seismic demands on isolators based on nonlinear analysis. J Struct Eng 2004;130(3):392–402.
[12] Van Nguyen D, Kim D, Nguyen DD. Nonlinear seismic soil-structure interaction analysis of nuclear reactor building considering the effect of earthquake frequency content. Structures: Elsevier; 2020. p. 901-14.
[13] Novak M, Henderson P. Base-isolated buildings with soil-structure interaction. Earthquake Eng Struct Dyn 1989;18(6):751–65.
[14] Tongaonkar NP, Jangid RS. Seismic response of isolated bridges with soil–structure interaction. Soil Dyn Earthquake Eng 2003;23(4):287–302.
[15] Krishnamoorthy A, Anita S. Soil–structure interaction analysis of a FPS-isolated structure using finite element model. Structures: Elsevier; 2016. p. 44-57.
[16] Tsiavos A, Haladij P, Sextos A, Alexander NA. Analytical investigation of the effect of a deformable sliding layer on the dynamic response of seismically isolated structures. Structures: Elsevier; 2020. p. 2426-36.
[17] Li C, Liu W, Wang S, Du D, Wang H. Shaking table test on high-rise isolated structure on soft soil foundation. J Build Struct 2013;34:72–8.
[18] Zhuang H, Fu J, Yu Xu, Chen Su, Cai X. Earthquake responses of a base-isolated structure on a multi-layered soft soil foundation by using shaking table tests. Eng Struct 2019;179:79–91.
[19] Ashiquzzaman M, Hong K-J. Simplified model of soil-structure interaction for seismically isolated containment buildings in nuclear power plant. Structures: Elsevier; 2017. p. 209-18.
[20] Almansa FL, Weng D, Li T, Alfarah B. Suitability of seismic isolation for buildings founded on soft soil. case study of a rc building in shanghai. Buildings 2020;10:241.;10(12):241. https://doi.org/10.3390/buildings10120241.
[21] Radkia S, Rahnavard R, Tuwair H, Gandomkar FA, Napolitano R. Investigating the effects of seismic isolators on steel asymmetric structures considering soil-structure interaction. Structures: Elsevier; 2020. p. 1029-40.
[22] Radkia S, Rahnavard R, Abbas GF. Evaluation of the effect of different seismic isolators on the behavior of asymmetric steel sliding structures. J Struct Construct Eng. 2019;6:213–30.
[23] Radkia S, Abbas Gandomkar F, Rahnavard R. Seismic response of asymmetric sliding steel structure with considering soil-structure interaction effects. J Struct Construct Eng. 2019;6:105–20.
[24] Anderson L, Ostadan F, Amin J, Carey S. Effect of separation distance and soil parameters on the structure-soil-structure interaction response of adjacent deeply embedded structures. 2013.
[25] Padrón LA, Aznárez JJ, Maeso O. Dynamic structure–soil–structure interaction between nearby piled buildings under seismic excitation by BEM–FEM model. Soil Dyn Earthquake Eng 2009;29(6):1084–96.
[26] Qian J, Tham LG, Cheung YK. Dynamic cross-interaction between flexible surface footings by combined bem and fem. Earthquake Eng Struct Dyn 1996;25(5):509–26.
[27] Trombetta N, Hutchinson T, Mason H, Zupan J, Bray J, Bolisetti C, et al. Centrifuge modeling of structure–soil–structure interaction: Seismic performance of inelastic building models. 15th world conference on earthquake engineering. 2012.
[28] Bolisetti C. Site response, soilstructure interaction and structure-soilstructure interaction for performance assessment of buildings and nuclear structures. State University of New York; 2014.
[29] Kirkwood P, Dashti S. A centrifuge study of seismic structure-soil-structure interaction on liquefiable ground and implications for design in dense urban areas. Earthquake spectra. 2018;34(3):1113–34.
[30] Çelebi M. Seismic responses of two adjacent buildings. II: Interaction. J Struct Eng 1993;119(8):2477–92.
[31] IS:1893-2016. Earthquake Resistant Design and Construction of Buildings Code of Practice: 1893-2016. Indian code.
[32] Basu D, Dey A, Kumar SS. One-dimensional effective stress non-Masing nonlinear ground response analysis of IIT Guwahati. International Journal of Geotechnical Earthquake Engineering (IJGEE). 2017;8:1-27.
[33] Deb SK, Dutta A. Verification test of a prototype base isolated two storeyed R.C.C. framed building subjected to actual earthquake. Rep No 2002/36/20/BRNS. 2007..
[34] Dubey PN, Reddy GR, Deb SK, Vaje KK, Ghosh AK, Kushwaha HS. Performance of base isolated RCC framed building under actual earthquake. Proceedings of the International Workshop on Earthquake Hazards and Mitigation. 2007.
[35] Nath RJ, Deb SK, Dutta A. Base isolated RC building-performance evaluation and numerical model updating using recorded earthquake response. Earthquakes Struct 2013;4(5):471–87.
[36] Midas G. NX user manual, Analysis Reference chapter 4 materials, Section 2. Plastic Mater Propert 2019.
[37] Kayal J. Seismicity of Northeast India and surroundings: Development over the past 100 years. J Geophys (Hyderabad). 1998;19:9–34.
[38] Sharma A, Jangid R. Behaviour of base-isolated structures with high initial isolator stiffness. Int J Appl Sci Eng Technol. 2009;5:199–204.
[39] Kothari P, Parulekar YM, Reddy GR, Gopalakrishnan N. In-structure response spectra considering nonlinearity of RCC structures: Experiments and analysis. Nucl Eng Des 2017;322:379–96.
[40] IS:456-2000. Plain and Reinforced Concrete. Indian code.
[41] Kim D-S, Stokoe K. Soil damping computed with Ramberg-Osgood-Masing Model. International conference on soil mechanics and foundation engineering1994. p. 211-4.
[42] Dammala PK, Kumar SS, Krishna AM, Bhattacharya S. Dynamic soil properties and liquefaction potential of northeast Indian soil for non-linear effective stress analysis. Bull Earthq Eng 2019;17(6):2899–933.
[43] Szilvágyi Z, Ray RP. Verification of the ramberg-osgood material model in midas GTS NX with the Modeling of Torsional Simple Shear Tests. Periodica Polytechnica Civil Eng 2018;62:629–35.
[44] Engineers ASoC. Seismic Analysis of Safety-Related Nuclear Structures. American Society of Civil Engineers; 2017.
[45] Hashash Y, Musgrove M, Harmon J, Groholski D, Phillips C, Park D. DEEPSOIL 6.1, user manual. Urbana, IL: Board of Trustees of University of Illinois at Urbana-Champaign; 2016.
[46] Rayhani MHT, El Naggar MH, Tabatabaei SH. Nonlinear analysis of local site effects on seismic ground response in the Bam earthquake. Geotech Geol Eng 2008;26(1):91–100.
[47] Das S, Gupta ID, Gupta VK. A probabilistic seismic hazard analysis of northeast India. Earthquake Spectra 2006;22(1):1–27.
[48] Gasparini D, Vanmarcke EH. SIMQKE: A program for artificial motion generation. Department of Civil Engineering, Massachusetts Institute of Technology, Cambridge, MA. 1976.